Abstract

Project Code: RSA6280101

Project Title: การศึกษาในหลอดทดลองและสัตว์ทดลองต่อบทบาทของ nuclear factor E2-related factor 2 (Nrf2) ในการควบคุมฤทธิ์เคอราติโนไซท์ต่อการปกป้องเมลาโนไซท์เพื่อพัฒนาสารยับยั้งความเสื่อมสภาพของ ผิวหนังรูปแบบอนุภาคระดับนาโน

Investigator: รศ. ดร. พญ.อุไรวรรณ พานิช

ภาควิชาเภสัชวิทยา คณะแพทยศาสตร์ศิริราชพยาบาลมหาวิทยาลัยมหิดล

E-mail Address: uraiwan.pan@mahidol.ac.th

Project Period: 3 years

บทคัดย่อ

รังสีอัลตราไวโอเลต (UVR) เป็นอันตรายต่อผิวหนังโดยทำให้เกิดความเสียหายต่อเซลล์ผิวหนังชนิด และเพิ่มความเสี่ยงต่อการพัฒนาเป็นมะเร็งผิวหนังทั้งชนิด non-melanoma และ melanoma รังสี UVA และ UVB เป็นอันตรายกับเซลล์ผิวหนังทั้งเซลล์ keratinocytes (เป็นเซลล์ส่วนใหญ่ที่ชั้น epidermis) เซลล์เมลาโน ไซท์ (melanocytes; MC) (เป็นเซลล์ระหว่างชั้น epidermis และ dermis ผลิตเม็ดสี melanin) และเซลล์ fibroblasts ซึ่งเกี่ยวข้องกับโครงสร้างผิวหนังและมีบทบาทต่อ skin aging โดยทำให้เกิดการทำลาย biomolecules (รวมทั้ง DNA, lipid และ protein) กระตุ้นการผลิต reactive oxygen species (ROS) ทำให้เกิด กาวะเครียดออกซิเดชั่น (oxidative stress) และรบกวนสัญญาณเซลล์ (cell signaling) รังสีอัลตราไวโอเลตบี (UVB) ทำให้เกิดการทำลายของดีเอ็นเอ (DNA damage) โดยตรง และมีผลต่อการตอบสนองของเซลล์ซึ่ง รวมถึงการตายของเซลล์ (apoptosis) และภาวะอักเสบ (inflammation) ในเซลล์ผิวหนัง ส่วนรังสี UVA สามารถ ผ่านชั้นผิวหนังเข้าไปถึงชั้น dermis เป็นปัจจัยภายนอกที่สำคัญทำให้เกิดภาวะผิวหนังเสื่อมสภาพจากแสงแดด (photoaging) โดยกระตุ้นการทำงานของเอนไซม์ matrix metalloproteinase-1 (MMP-1) ทำให้เกิดการย่อย และทำลายคอลลาเจน (collagen degradation) ทำให้เกิดความเสียหายของโครงสร้างผิวหนังเป็นริ้วรอย (wrinkle formation) ซึ่งเป็นลักษณะสำคัญของภาวะ skin aging

เซลล์ผิวหนังสามารถมีปฏิกิริยาระหว่างเซลล์ต่างชนิด (cell interaction) ผ่านการหลั่งโปรตีน paracrine factors ผู้วิจัยได้พัฒนา model ของเซลล์ผิวหนังที่เพาะเลี้ยงร่วมกัน (co-culture) ที่สามารถสะท้อนสรีรวิทยา ของผิวหนังที่ใช้ในการศึกษาความสัมพันธ์ระหว่างเซลล์ผิวหนังที่มีบทบาทต่อการควบคุมหน้าที่และโครงสร้าง ของผิวหนัง โครงการวิจัยนี้จึงใช้การศึกษาการแสดงออกของยืนเชิงระบบ (transcriptome analysis) เพื่อค้นหา พาราครินที่สำคัญ (candidate paracrine factors) ที่หลั่งจาก KC ที่มีบทบาทควบคุมการตอบสนองของ MC ต่อรังสี UVB ในเซลล์ผิวหนังเพาะเลี้ยงและผิวหนังหนู (in vitro and in vivo skin models)

Nuclear factor erythroid 2-related factor 2 (Nrf2) เป็น transcription factor สำคัญที่ควบคุมการ แสดงออกระดับยีนของ antioxidant defense และกลไกกระตุ้นการทำงาน Nrf2 ยังเกี่ยวข้องกับการทำงานของ ไมโทคอนเดรีย (mitochondria) ซึ่งมีหน้าที่สำคัญในการผลิตพลังงานภายในเซลล์ และปกป้องเซลล์ผิวหนังจาก รังสี UV ดังนั้นการกระตุ้นการทำงานของ Nrf2 และ mitochondria ที่ควบคุมระบบต้าน oxidation (Nrf2-regulated redox homeostasis) จึงเป็นแนวทางทางเภสัชวิทยาที่สำคัญในพัฒนาสารยับยั้งความเสื่อมสภาพ ของผิวหนัง (anti-photoaging agent) ที่มีประสิทธิภาพ

นอกจากนี้การใช้นวัตกรรมนาโนเทคโนโลยีในการขนส่งยาระดับนาโน (nanoparticle based-targeted drug delivery) จะช่วยเพิ่มประสิทธิภาพการขนส่งของสารออกฤทธิ์ไปยังเซลล์ผิวหนังเป้าหมายได้ ดังนั้นทีม ผู้วิจัยจึงมีวัตถุประสงค์ในการพัฒนาสารสมุนไพรที่บรรจุในอนุภาคระดับนาโนรูปแบบทาผิว และทดสอบฤทธิ์ anti-photoaging ที่บรรจุในอนุภาคระดับนาโนในผิวหนังหนู ทีมผู้วิจัยยังพบว่าสารสกัดสมุนไพรตำรับ อายุรเวทศิริราชห้าราก (HRF) ที่มีการใช้อย่างแพร่หลายตั้งแต่อดีต และสาร phytochemicals ที่เป็นสารออก ฤทธิ์ในพืชและสมุนไพร ได้แก่ sulforaphane (SFN) มีฤทธิ์ยับยั้ง photooxidative stress ในเซลล์ผิวหนังผ่าน การกระตุ้นการทำงานของ Nrf2 โครงการวิจัยนี้จึงพัฒนา HRF ในรูปแบบทาด้วยการใช้นาโนเทคโนโลยีใน การขนส่งยาระดับนาโน (nanoparticle based-targeted drug delivery) และศึกษาฤทธิ์ยับยั้งความเสื่อมสภาพ (anti-aging) ของ HRF ที่บรรจุในอนุภาคระดับนาโนรูปแบบทาผิว (nanoparticle-based topical HRF) ใน ผิวหนังหนูที่ถูกกระตุ้นให้เกิดการเสื่อมสภาพจากรังสีอัลตราไวโอเลตชนิดเอ (UVA) ผู้วิจัยคาดว่าโครงการวิจัย นี้จะนำไปสู่การค้นพบ candidate paracrine factors ที่หลั่งจาก KC ที่มีบทบาทควบคุมการตอบสนองของ MC ต่อรังสี UVB ซึ่งสามารถต่อยอดสู่การพัฒนา biomarkers ที่สามารถใช้ในเกี่ยวกับการทำนาย (prediction) ความเสี่ยงการเกิดโรคทางผิวหนังที่เกิดจากรังสี UV รวมทั้งมะเร็งผิวหนังเพื่อเพิ่มประสิทธิภาพในการป้องกัน โรค และพัฒนาแนวทางการรักษาใหม่ที่มีประสิทธิภาพและความปลอดภัย นอกจากนี้การพัฒนาสารสกัด สมุนไพรและสารกลุ่ม phytochemicals รูปแบบอนุภาคระดับนาโนสามารถต่อยอดสู่ผลิตภัณฑ์ชะลอความ เสื่อมสภาพของผิวหนังที่มีประสิทธิภาพและความปลอดภัย

Abstract

Skin microenvironment created by keratinocytes (KC) can influence stress responses of melanocytes (MC) to UVB insult. Here, we investigated interactions of the microenvironment created by KC and MC by identifying paracrine factors derived from KC using RNA sequencing analysis and determining the role of the identified paracrine factors in modulating the UVB-mediated MC responses. We found that G-CSF and CCL20 were upregulated in UVB-irradiated KC and their expression levels best correlate with the protective effects of KC-derived conditioned media on MC responses to UVB. Treatment with recombinant G-CSF and CCL20 revealed the strongest modulatory effects on UVB-induced MC responses by mitigating apoptosis and oxidative stress as well as stimulating melanogenesis. Similar correlation between G-CSF and CCL20 expression in KC and the tyrosinase level in MC was also observed in the UVB-irradiated mouse skin. Our result thus identifies for the first time that G-CSF and CCL20 are important paracrine factors secreted from KC that play a regulatory role in UVB-mediated MC damage, that could provide translational insights for the development of biomarkers for predicting susceptibility to photodamage.

Since mitochondria are the major source of oxidant production as well as key sources of cellular oxidants during UVA exposure, we also demonstrated that the two potent novel mitochondria-targeted H₂S delivery molecules (AP39 and AP123) exerted anti-photoaging effects via preserving mitochondrial bioenergetics with concomitant increases in Nrf2 activity. Therefore, our study suggested that natural and synthetic compounds targeting Nrf2 and mitochondria may represent a promising pharmacological strategy for the prevention and treatment of skin photoaging.

Recently, nanotechnology has gained prominence and emerged as a more effective way of treatment for skin by topical administration because nanoparticles-based topical delivery system can improve the efficiency of topical delivery of candidate compounds. Nanoparticles using polymer nanoparticles, poly (lactic-co-glycolic acid) (PLGA), has been approved by the US Food and Drug Administration (FDA) for the use of drug delivery. In this study, we also developed the HRF (Harak formula) and its bioactive hispidulin (HPD)-loaded polylactide-co-glycolide (PLGA) nanoparticles (HRF-NPs and HPD-NPs, respectively) and investigated their anti-photoaging effects compared to free HRF and HPD controls through the inhibition of MMP-1 and promotion of collagen in mouse skin. Our study demonstrated that treatment with HRF-NPs significantly protected against UVA-induced oxidant generation NHDFs. Moreover, topical administration of HRF-NPs 1 h prior to UVA exposure (accumulation dose of 60 J/cm²) mitigated an increase in MMP-1 protein expression and decrease in collagen type I protein expression in UVA-irradiated mouse skin. At an equal amount of the compound mass, less quantity of HRF by approximately 50% in nanoparticle-based formulation compared to free HRF control had abilities to suppress UVA-induced skin photoaging in association with inhibition of cellular oxidant formation.

Our study concludes that the microenvironment created by KC played a regulatory role on the stress responses of MC to UVB via paracrine actions mediated by GCSF and CCL20. Promotion of Nrf2 activity by medicinal plants (HRF extracts) and their bioactive compounds (e.g., HPD) as well as targeting H₂S delivery to mitochondria may represent a promising pharmacological strategy for the prevention and treatment of skin photoaging. Furthermore, PLGA nanoparticles improved the efficiency of HRF in protection against UVA-induced skin photoaging. Further investigations on clinical efficacy and safety are required to develop of the HRF encapsulated in PLGA-based nanoparticles as promising anti-photoaging agents.

Keywords: paracrine factor, photoaging, oxidative stress, nuclear factor E2-related factor 2 (Nrf2), Harak formula-based nanoparticles (HRF-NPs)

เนื้อหาวิจัย

(1) วัตถุประสงค์ของโครงการ

- To identify the candidate paracrine factors secreted by KC responsible for their protective effects on UVB-mediated MC responses using systems approaches (transcriptomic and protein array-based analysis).
- 2) To investigate the role of the candidate paracrine factors in UVB-induced oxidative stress, apoptosis and melanogenesis in MC treated with conditioned medium (CM) from KC
- 3) To develop topical-based nanoparticles incorporated with Nrf2 inducers as potential antiphotoaging agents that target the candidate paracrine factors of KC using a mouse model of photoaging.

(2) ระเบียบวิธีวิจัย

<u>Part I.</u> To identify the candidate paracrine factors secreted by KC responsible for their protective effects on UVB-mediated MC responses using transcriptome analysis.

2.1 Cell culture

Primary human epidermal melanocytes (MC) and primary human epidermal keratinocytes (KC) were obtained from Invitrogen (NY, USA). MC were cultured in Medium 254 (#M-254-500) supplemented with human melanocyte growth supplement (HMGS) according to the manufacturer's instructions. Primary human epidermal keratinocytes (KC) were cultured in Medium 154 (#M-154CF-500) supplemented with human keratinocyte growth supplement (HKGS). Human keratinocyte (HaCaT) cells (Cell Lines Service, Heidelberg, Germany) were grown in high glucose (4.5 g/L) Dulbecco's modified Eagle's medium (DMEM) and Ham's F-12 (DMEM/F-12) supplemented with 10% fetal bovine serum and 1% penicillin (100 U/ml)/streptomycin (100 mg/ml). Primary human dermal fibroblast (HDF) were grown in high glucose (4.5 g/L) Dulbecco's modified Eagle's medium (DMEM) supplemented with 10% fetal bovine serum, 1% 200 mM glutamax and 1% Antibiotic-Antimycotic Solution (Mediatech, Inc. Manassas, VA). Primary mouse embryonic fibroblast cells (NIH3T3) and epidermoid carcinoma (A431) were cultured in Dulbecco's minimal essential media (DMEM) supplemented with 10% fetal bovine serum and 1% Antibiotic-Antimycotic Solution (Mediatech, Inc. Manassas, VA). All cells were maintained at 37 °C in a humidified air of 5% CO2 (PCO2 = 40 Torr) (a Forma Scientific CO2 Water Jacketed Incubator).

2.2 Preparation of cell-derived conditioned medium (CM)

KC, HaCaT, HDF, NIH3T3 and A431 were seeded at a density of 5 × 10⁵ cells/well in 6 cm² dishes. Conditioned-KC, HaCat, HDF, NIH3T3 and A431 supernatants were prepared by irradiation of 5 skin cells in DPBS with UVB (125 mJ/cm²) and the DPBS were changed to DMEM medium and collected at 12 h post-irradiation and used as KC-CM, HaCat-CM, HDF-CM, NIH3T3-CM and A431-CM for treatment of MC. MC were pre-incubated with KC-CM, HaCat-CM, HDF-CM, NIH3T3-CM and A431-CM for 30 min, subjected to UVB irradiation and harvested at 1 h following 62.5 mJ/cm² UVB irradiation for determination of ROS formation, 12 h after 250 mJ/cm² irradiation for caspase-3 activation and 12 h after 125 mJ/cm² irradiation for melanin content, tyrosinase activity.

2.3 Recombinant paracrine factor treatment

The stock solution of recombinant paracrine factors was prepared in distilled water. In all experiments, the stock solutions were then diluted in the serum free DMEM. The four different concentrations, 0.3, 1, 3 and 9 nM, of 14 recombinant paracrine factors including Granulocyte colony-stimulating factor (GCSF), Chemokine (C-C motif) ligand 20 (CCL20), Endothelin1 (ET-1), Placental growth factor (PIGF), chemokine (C-X-C motif) ligand 8 (CXCL8), TNF Receptor Superfamily Member 10b (TNFRSF10B), Chemokine (C-X-C motif) ligand 2 (CXCL2), Interleukin 6 (IL-6), Interleukin 16 (IL-16), Bone morphogenetic protein 2 (BMP2), Persephin (PSPN), Interleukin 36 gamma (IL36G), Epiregulin (EREG), Dickkopf-related protein (DKK1) were used. MC were preincubated with KC-CM and 14 recombinant paracrine factors for 2 h, subjected to UVB irradiation and harvested at 12 h following 250 mJ/cm² UVB irradiation for determination of caspase-3 activation and 12 h after 125 mJ/cm² irradiation for melanin content.

2.4 UVB irradiation

MC, KC, HaCaT, HDF, NIH3T3 and A431 cells were irradiated with UVB under a thin layer of Dulbecco's phosphate buffered saline (DPBS). The UV intensity determined at a distance of 21 cm from the UVR lamp was 1 W/cm2 using a UV-meter (Dr Honle, Martinsried, Germany). The culture plates were exposed for 22.5, 45 s or 1 min 30 s to achieve a single dose of 62.5, 125 or 250 mJ/cm2, respectively. Immediately after UVB exposure, DPBS were replaced with Medium 254 without HMGS for MC and DMEM without FBS for KC, HaCaT, HDF, NIH3T3 and A431. MC were harvested at 1 h post-irradiation for ROS formation and 12 h post-irradiation for apoptosis using cleaved caspase-3 assays, melanin content and tyrosinase activity. KC, HaCaT, HDF cells were harvested at 6 h post-irradiation for mRNA expression.

2.5 Determination of intracellular oxidant formation by flow cytometry

DCFH-DA were used to determine intracellular reactive oxygen species (ROS). The principle of DCFH-DA method is detecting the intensity of green fluorescence that occur after deacetylation and subsequent oxidation product of probe. DCFH-DA gets into cells and accumulates mainly in cytosol, and then it was hydrolyzed in the cells to DCFH, further oxidized by oxidants (e.g., H_2O_2) in the cells to fluorescent 2,7-dichlorofluorescein (DCF). Thus, the fluorescence reflected the overall oxidative stress and oxidant formation in cells which can be visualized and detected by using FACS Calibur. The assay is based on conversion of non-fluorescent dichlorofluorescein (H2DCFDA) to the fluorescent 2,7-DCF upon oxidation by intracellular ROS. After a 1 h period of UVB irradiation, MC were washed. Then, cells were incubated in DPBS with 20 μ M H_2 DCFDA at 37 °C for 30 min and analysed by flow cytometery using a fluorescence activated cell sorter (FACS-calibur).

2.6 Measurement of active caspase-3

Caspase-3 is crucial mediator of programmed cell death (apoptosis). In apoptotic cell, caspase3 can be activated both by extrinsic (death ligand) and intrinsic (mitochondrial) pathways. In cells undergoing apoptosis, caspase-3 is a key protease that is activated during the early stages of apoptosis and synthesized as an inactive pro-enzyme. Active caspase-3 were measured using PE Active Caspase-3 Apoptosis Kit (BD Biosciences, USA) according to the manufacturer's instructions. After a 12 h period of UVB irradiation, MC were washed for determination of active caspase-3. Briefly, MC were fixed and permeabilized using the Cytofix/CytopermTM for 30 min, pelleted and washed with Perm/Wash TM Buffer. Cells were subsequently stained with the rabbit anti-active caspase-3 antibody (clone C92-605) (BD Biosciences, USA) in the dark. Cells were then washed and resuspended in Perm/WashTM Buffer and analyzed by flow cytometry.

2.7 Determination of melanin content and tyrosinase activity

Melanin content and tyrosinase activity were determined in MC. Cells harvested at 12 h post irradiation. The melanin and tyrosinase activity monitored by dopachrome formation were measured spectrophotometrically at 475 by a spectrophotometer. The amount of melanin (μ g/mg protein) was calculated by comparing with a standard curve generated using synthetic melanin. The tyrosinase activity (unit/mg protein) was calculated by comparison to a standard curve using tyrosinase (2034 U/mg).

2.8 Quantitative real-time reverse transcriptase-polymerase chain reaction (RT-PCR) for determination of mRNA expression

Expressions of CRH, CRHR1, ET-1 and POMC mRNA were determined by RT-PCR. Total RNA was isolated using the illustra RNAspin Mini RNA Isolation Kit (GE Healthcare, UK) and reverse transcription was carried out using the Improm-II reverse transcriptase (Promega, Medison, USA)

under the conditions described in the kit manual. Primers for PCR were designed using the Primer Express software version 3.0 (Applied Biosystems, USA). Sequences of PCR primer (in 5'→3' direction) were as follows: CRH (product sizes = 144 bp) sense, CTCCGGGAAGTCTTGGAAAT, and antisense, GTTGCTGTGAGCTTGCTGTG; CRHR1 (product sizes = 100 bp) sense, TGGATGTTCATCTGCATTGG, and antisense, TGCCAAACCAGCACTTCTC; ET-1 (product sizes = 274 bp) sense, TCTACTTCTGCCACCTGGAC, and antisense, CACTTCTTTCCCAACTTGGAAC; POMC, exon 3 (product sizes = 152 bp) sense, AGCCTCAGCCTGCAA, and antisense, CAGCAGGTTGCTTTCCGTGGTG. The mRNA level was calculated by normalizing with the expression level of GAPDH mRNA. The mean Ct from mRNA expression in cDNA from each sample was compared with the mean Ct from GAPDH determinations from the same cDNA samples.

2.9 RNA sequencing analysis (RNA-seq)

RNA samples were prepared using Trizol, purified by Ambion RNA isolation kit (Invitrogen) and treat with PureLink DNase set (Invitrogen). The integrity of RNA was analyzed by running on agarose gel electrophoresis and measuring RIN value by Agilent 2100 Bioanalyzer (Agilent Technologies). All samples showed high integrity of RNA with intact 28sRNA, intact 16sRNa and RNA integrity number (RIN)>8. Total RNA of each sample was quantified and qualified by Agilent 2100 Bioanalyzer (Agilent Technologies, Palo Alto, CA, USA), NanoDrop (Thermo Fisher Scientific Inc.) and 1% agarose gel. 1 g total RNA with RIN value above 7 was used for following library preparation. Next generation sequencing library preparations were constructed according to the manufacturer's protocol (NEBNext® Ultra™ RNA Library Prep Kit for Illumina®). The poly(A) mRNA isolation was performed using NEBNext Poly(A) mRNA Magnetic Isolation Module (NEB). The mRNA fragmentation and priming were performed using NEBNext First Strand Synthesis Reaction Buffer and NEBNext Random Primers. First strand cDNA was synthesized using ProtoScript II Reverse Transcriptase and the second-strand cDNA was synthesized using Second Strand Synthesis Enzyme Mix. The purified (by AxyPrep Mag PCR Clean-up (Axygen)) double-stranded cDNA was then treated with End Prep Enzyme Mix to repair both ends and add a dA-tailing in one reaction, followed by a T-A ligation to add adaptors to both ends. Size selection of Adaptor-ligated DNA was then performed using AxyPrep Mag PCR Clean-up (Axygen), and fragments of ~360 bp (with the approximate insert size of 300 bp) were recovered. Each sample was then amplified by PCR for 11 cycles using P5 and P7 primers, with both primers carrying sequences which can anneal with flow cell to perform

bridge PCR and P7 primer carrying a six-base index allowing for multiplexing. The PCR products were cleaned up using AxyPrep Mag PCR Clean-up (Axygen), validated using an Agilent 2100 Bioanalyzer (Agilent Technologies, Palo Alto, CA, USA), and quantified by Qubit 2.0 Fluorometer (Invitrogen, Carlsbad, CA, USA). Then libraries with different indices were multiplexed and loaded on an Illumina HiSeq instrument according to manufacturer's instructions (Illumina, San Diego, CA, USA). Sequencing was carried out using a 2x150bp paired-end (PE) configuration; image analysis and base calling were conducted by the HiSeq Control Software (HCS) + OLB + GAPipeline-1.6 (Illumina) on the HiSeg instrument. Sequencing was performed on the Illumina HiSeg platform, in a 2x150bp paired-end (PE) configuration, with 2.0 Gb raw data per sample. Basecalling was performed by Illumina RTA software in sequencer, further demultiplexing was performed by Illumina bcl2fastq 2.17 software based on index information, the number of reads and quality score (Q30) were counted as well. Alignment of reads to the human reference (hg19) was done using STAR version v2.5.3a (1) on Basepair website (https://www.basepairtech.com/). Other pipelines were used including 'sambamba' (v0.6.6) (2) for sorting the BAM files, 'samtools' (v1.6) (3) for indexing the BAM files, 'fastp' (v0.19.4) (4) for the read trimming and QC and 'subread' (v1.6.2) (5) for the gene/isoform quantification. Trimming of low-quality base pair was done using Phred quality score (Q score) at 10 as the cut-off. (6) Differential gene expression was done using BioJupies platform (https://biojupies.cloud). (7) Significant level was considered if adjusted p-value < 0.05.

2.10 Determination of GCSF levels by ELISA

GCSF levels in culture supernatants were determined using competitive enzyme immunoassay kits from DCS50, R&D Systems, Inc., USA, according to the manufacturer's instructions. Sample or GCSF standards were added to the immunoplate pre-coated with secondary antibody. An anti-GCSF antibody was added, followed by biotinylated peptide. Biotinylated peptide then interacted with streptavidin-horseradish peroxidase (HRP), which catalyzed the substrate solution.

2.11 Determination of UVR-induced cell damage in vivo

Three-week-old female BALB/c wild-type mice were purchased from National Laboratory Animal Center, Mahidol University and maintained under controlled conditions (25 ± 2 °C with 55 ± 5 % relative humidity in a 12-h light:12-h dark cycle) using an isolator caging system. Water and food diet were available ad libitum during the experimental period. Mice were randomized into 4 groups of 4 mice. Group I (control), without UVB exposure. Group II, UVB 2 time of 250 mj/cm² irradiation

(a cumulative total dose of 500 mJ/cm²). Group III, UVB 3 time of 250 mj/cm² irradiation (a cumulative total dose of 750 mJ/cm²). Group IV, UVB 3 time of 250 mj/cm² irradiation (a cumulative total dose of 1000 mJ/cm²). Mice were anesthetized by an intraperitoneal injection (*i.p.*) of 100:10 mg/kg of ketamine/xylazine cocktail. Dorsal skin was removed at 12 h after last exposure of UVB, embedded in Tissue-Tek® OCT compound and directly snap-frozen (liquid N₂), and stored at =80 °C until microtome sectioning. Skin thickness was assessed by hematoxylin and eosin (H&E) and immunofluorescence (IF) staining. CCL20, GCSF, tyrosinase, pan-cytokeratin (keratinocyte marker) and gp100 (melanocyte marker) were assessed by immunofluorescence and DAPI was used to counterstain nuclei. Image analysis was performed using Image J.

<u>Part II</u> *In vivo* study on the anti-photoaging effects of mitochondria-targeted molecules, herbal extracts (Harak formula), Nrf2 inducers and topical-based nanoparticles incorporated with medicinal plants (Harak formula) and its bioactive

2.12 Animal model and the treatment

All animal experiments were reviewed and approved by the Siriraj Animal Care and Use Committee (SiACUC), SiACUP 023/2557. BALB/c mice were obtained from the National Laboratory Animal Center, Mahidol University and were housed under standard housing conditions with light: dark cycle at 12:12 hours. BALB/c mice (4-5 weeks of age with an average body weight of 20 grams) were anesthetized by intraperitoneal injection of a ketamine (80 mg/kg)/ xylazine (10 mg/kg) cocktail. The dorsal surfaces were then shaved on using an electric hair clipper (Remington, PG-180). The scarified area was cleansed with a cotton-tipped applicator saturated with sterile normal saline solution. The novel mitochondria-targeted hydrogen sulfide (H2S) donors AP39 and AP123, harak formula (HRF) extracts at the concentrations of 10, 30 and 100 mg/cm², hesperitine (HSP) at the concentrations of 0.3, 1, and 3 mg/cm² and sulforaphane (SFN) at 0.1 mg/cm² were obtained to perform in all biomarkers of the in vivo study. We also developed the HRF (Harak formula) and and its bioactive hispidulin (HPD)-loaded polylactide-co-glycolide (PLGA) nanoparticles (HRF-NPs and HPD-NPs, respectively) and tested the anti-photoaging effects of HRF-PLGA-NPs and free HRF at 5, 15, 50 mg/cm² as well as HPD-PLGA-NPs and free HPD at 6, 20, 60 mg/cm² compared to free HRF and HPD controls on mouse skin. The test samples were topically administered to each 1-cm² site in the center area of the shaved dorsal skin 1 h prior to each UVA exposure. The mice were exposed to UVA irradiation for 10 minutes to achieve a single dose of 10 J/cm², 3 times a week for 2 weeks (60 J/cm² in total). The dorsal skin flaps were then removed at different time points. Skin thickness was assessed by hematoxylin and eosin (H&E) and immunofluorescence (IF) staining. Photoaging markers MMP-1 and collagen, oxidative DNA damage (8-OHdG), as well as Nrf2 nuclear accumulation and the protein levels of its downstream target genes GST and NQO-1, were assessed by IF. The timeline of treatment, the UVA dose selection, procedures of immunofluorescence (IF) staining protocol and all analysis of the protein expression data were described below following previous reports (Shimada et al., 2011; Chaiprasongsuk et al., 2017).

2.13 Hematoxylin and eosin (H&E) analyses of skin thickness

Frozen tissues were sectioned by using Cryostat (Thermo scientific, USA) for 8 μ m per 1 section. Cryo-cut tissue sections were fixed in ice-cold acetone and air-dried for 30 min at room temperature. H&E staining was performed for histological evaluation of skin thickness as previously described in Chaiprasongsuk et al., 2017. Briefly, tissue sections were washed in distilled water for 2 min, incubated with hematoxylin for 4 min, and then washed in distilled water for 10 min. The slides were then incubated with eosin for 1 min and 95% alcohol for 1 min. The slides were dehydrated with 95% alcohol, 2 changes of absolute alcohol and acetone as well as 3 changes of xylene. An inverted fluorescent microscope equipped with a Nikon Intensilight was used for the imaging of H&E staining which was quantified using ImageJ software (Gawronska-Kozak et al., 2016; Chaiprasongsuk et al., 2017).

2.14 Immunofluorescence analysis of Nrf2 nuclear translocation and its target proteins (GST, and NQO-1), oxidative DNA damage, MMP-1, collagen

Dorsal skin tissue samples were collected at various time points following the final UVA irradiation; 1 and 6 h post-irradiation for Nrf2 and its target proteins, respectively; 1 h post-irradiation for oxidative DNA damage; 24 h post-irradiation for MMP-1 and collagen. Tissue sections were washed with PBS for 5 min/time (3 times) and blocked with phosphate-buffered saline (PBS) containing 2% BSA for 30 min. After removing excess blocking buffer, the slides were incubated with Nrf2 Ab (ab31163; Abcam, Cambridge, MA, USA), GST Ab (sc-459; Santa Cruz Biotechnology, Santa Cruz, CA), NQO1 Ab (ab34173; Abcam, Cambridge, MA, USA) (1:50), 8-OHdG [N45.1] Ab (ab48508; Abcam, Cambridge, MA, USA) (1:50), MMP-1 Ab (ab137332; Abcam, Cambridge, MA, USA) (1:50), collagen I (C-18) Ab (sc-8784; Santa Cruz Biotechnology, Santa Cruz, CA) (1:50) for 1 h. The slides were then washed for 5 min/time (3 times) with a PBS solution and incubated for 1 h at room temperature with FITC-conjugated the secondary Ab (green) and with DAPI (blue) to counterstain the nuclei for detection of nuclear Nrf2, the secondary Ab Alexa Fluor 488 goat anti-rabbit (Abcam) for detection of MMP-1, collagen, and phosphorylated protein levels. An inverted fluorescent microscope equipped with a Nikon Intensilight was used for the imaging of immunofluorescence (IF) stainings (20X) which were quantified using ImageJ software.

2.15 Data analysis

ImageJ software (NIH, Rockville, MD, USA was used to quantify the immunoblot intensity, thickness, and the IF intensity of the protein expressions. For all analysis of protein expression data, the corrected total cryosection fluorescence (CTCF) was calculated using the following equation: CTCF = integrated density – (area of each region of interest (ROI) × mean fluorescence of background readings) and the data were presented as percentage of control. Quantitative fluorescence analysis from ImageJ was then imported into Microsoft Excel to create histograms for further analysis. All analysis of protein expression data was presented as a percentage of control. The Nrf2 nuclear localization was analyzed based on the ratio of fluorescence intensity in the nuclear (indicated by the DAPI staining) to cytoplasmic intensity of Nrf2 (N/C ratio). Background subtraction was done to correct the intensity from each compartment (Noursadeghi et al., 2008; Chaiprasongsuk et al., 2017).

2.16 Statistical analysis

Data for *in vitro* study were reported as means \pm standard deviation from at least three biological replicates ($n \ge 3$) performed on different days using freshly prepared reagents. The significance of non-irradiated controls or individual treatment groups in comparison to the UVA-irradiated groups was evaluated by independent *t*-test (Student's; 2 populations) or one-way analysis of variance (ANOVA) followed by Tukey or Dunnett tests, where appropriate, using Prism (GraphPad Software Inc., San Diego, CA). Data for *in vivo* study are reported as means \pm SD. The significance of non-irradiated controls or sham controls or individual treatment groups in comparison to the shamirradiated mice was evaluated by independent *t*-test (Student's; 2 populations) or one-way ANOVA followed by Tukey or Dunnett tests, where appropriate.

3. ผลงานวิจัยที่ได้รับ

3.1 The paracrine protective effects on UVB-induced apoptosis of MC

At first, paracrine actions of 5 types of the skin cells keratinocytes (KC), human keratinocyte cell line (HaCaT), primary human dermal fibroblasts (HDF), mouse fibroblast cell line (NIH3T3) and epidermoid carcinoma (A431) cells were stimulated by exposure of the cells to UVB irradiation (125 mJ/cm²). The protective effects of KC, HaCaT, HDF, NIHT3T, A431 cells on UVB-induced apoptosis were assessed in melanocytes (MC) treated with conditioned medium (CM) from KC, HaCaT, HDF, NIHT3T, A431 cells. UVB irradiation markedly stimulated caspase3 activation (Fig. 1A) in MC alone. However, UVB-mediated active caspase-3 was remarkably reduced in MC treated with CM from KC, HaCaT, HDF and NIH 3T3 compared to MC alone in response to UVB irradiation. In addition, the results demonstrated that KC provided protective effect for inhibition of caspase3 activation in MC greater than other cell types. We next investigated the protective effects of different cell ratios of KC, HaCaT, HDF on UVB-induced caspase3 activation in MC at 12 h after UVB irradiation. MC were treated MC with CM from KC, HaCaT, HDF at three cell ratios (1:2.5, 1:5, 1:10). The results observed that different cell ratios caused different extents of paracrine actions. The cell ratios 1:5 and 1:10 provided significantly protective effect against UVB-mediated apoptosis of MC (Fig. 1B).

3.2 The paracrine protective effects on UVB-induced reactive oxygen species (ROS) formation in MC

All skin cells were exposed to UVB irradiation (125 mJ/cm²) to produce paracrine action. At 12 h post-irradiation, conditioned medium (CM) from KC, HaCaT, HDF, NIHT3T, A431 cells were collected and then their protective effects against UVB-induced ROS formation were assessed in MC treated with conditioned medium (CM) from each skin cell type. UVB irradiation was observed to cause induction of oxidant formation (Fig. 2) in MC alone, decreased oxidant formation were found in MC treated with CM from KC, HaCaT, HDF, NIH 3T3 except A431 compared to MC alone in response to UVB irradiation. In addition, the results demonstrated that KC provided the highest modulatory effects on UVB-induced oxidant formation in MC.

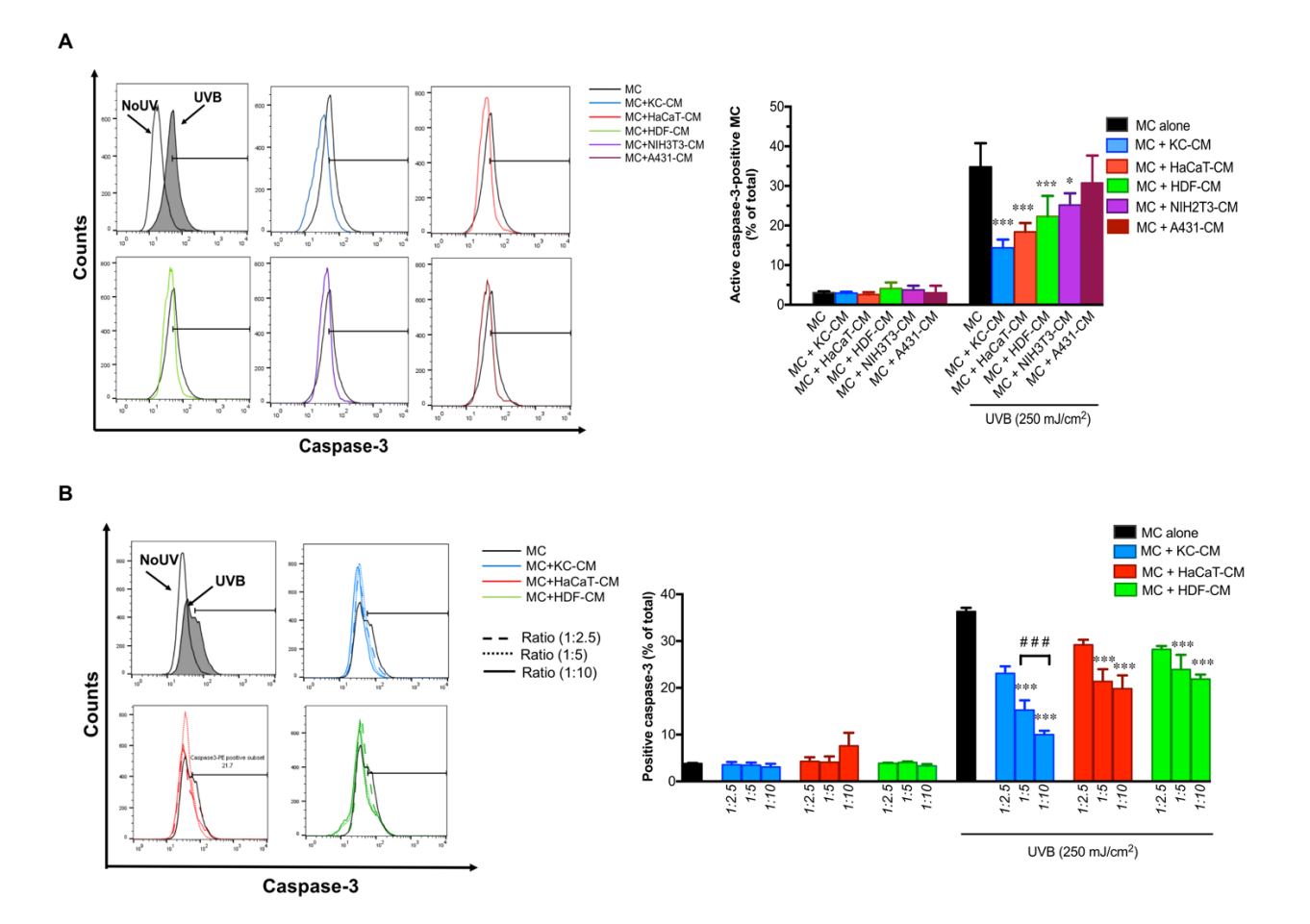
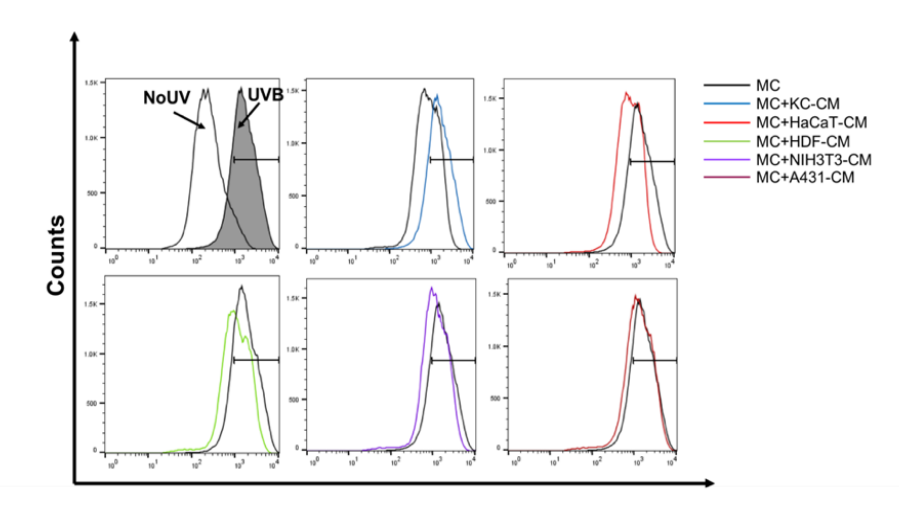


Fig 1. The protective effects of KC, HaCaT, HDF, NIHT3T, A431 cells on UVB (250 mJ/cm²)-induced apoptosis in MC treated with conditioned (CM) from KC, HaCaT, HDF, NIHT3T, A431 cells. The effects of UVB on caspase3 activation in MC pretreated with CM from KC, HaCaT, HDF, NIHT3T, A431 irradiated with UVB (125 mJ/cm²) for 30 min at 12 h after UVB irradiation. (A). The statistical significance of differences between UVB-irradiated MC and UVB-irradiated MC+KC-CM, MC+HaCaT-CM, MC+HDF-CM, MC+NIH3T3-CM and MC+A431-CM was evaluated by one-way ANOVA followed by Dunnett's test (*P < 0.05; ***P < 0.001 versus UVB-irradiated MC). The effects of different cell ratios of KC, HaCaT, HDF on UVB-induced caspase3 activation in MC at 12 h after UVB irradiation. MC were treated with CM from KC, HaCaT, HDF at three cell ratios (1:2.5, 1:5, 1:10). The statistical significance of differences between UVB-irradiated MC and UVB-irradiated MC+KC-CM, MC+HaCaT-CM, MC+HDF-CM at different cell ratios was evaluated by one-way ANOVA followed by Dunnett's test (***P < 0.001 versus UVB-irradiated MC). ### P < 0.001versus UVB-irradiated MC+KC-CM at cell ratio (1:5)



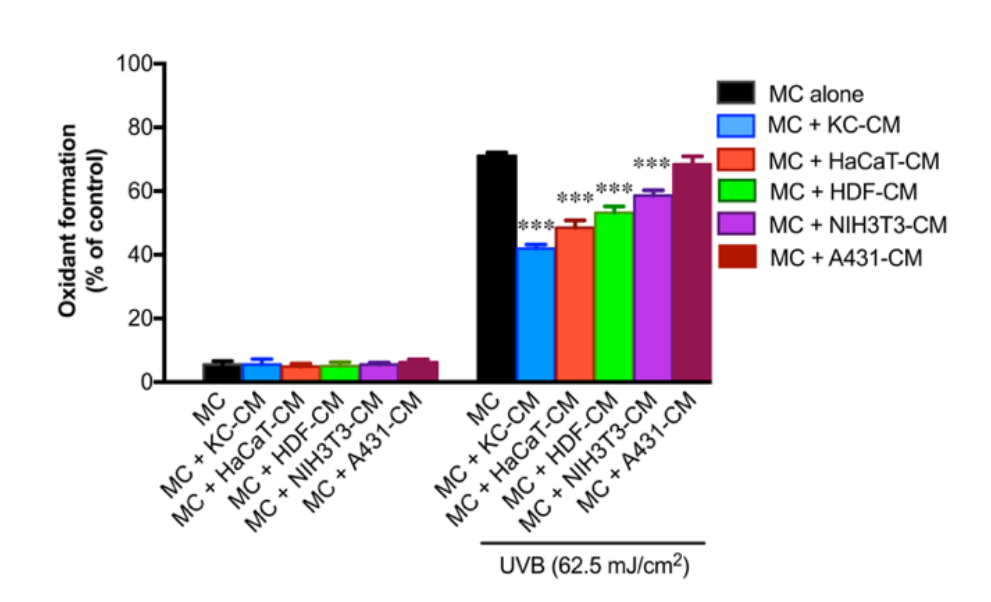


Fig 2. The protective effects of KC, HaCaT, HDF, NIHT3T, A431 cells on UVB (62.5 mJ/cm2)-induced ROS formation in MC treated with CM from KC, HaCaT, HDF, NIHT3T, A431 cells. The effects of UVB on ROS formation in MC pretreated with CM from KC, HaCaT, HDF, NIHT3T, A431 irradiated with UVB (125 mJ/cm²) for 30 min. The statistical significance of differences between UVB-irradiated MC and UVB-irradiated MC+KC-CM, MC+HaCaT-CM, MC+HDF-CM, MC+NIH3T3-CM and MC+A431-CM was evaluated by one-way ANOVA followed by Dunnett's test (***P < 0.001 versus UVB-irradiated MC).

3.3 The paracrine protective effects on UVB-induced melanogenesis in MC

Skin cell responses to UVB irradiation by increased melanin synthesis and tyrosinase. We observed that UVB irradiation activated melanin content (Fig. 3A) and tyrosinase activity (Fig. 3B) in MC, increased melanin content and tyrosinase activity were observed in MC treated with CM from KC, HaCaT, HDF, NIH3T3 compared to MC alone in response to UVB irradiation. In addition, the results demonstrated that CM from KC gave the strongest action in induction of melanin content and tyrosinase activity induced by UVB irradiation. We also explored heatmap analysis to conclude the paracrine protective effects on UVB-induced apoptosis, ROS formation and melanogenesis in MC (Fig. 4). The results showed that CM from 4 types of the skin cells (including KC, HaCaT, HDF and NIH3T3) were able to suppress caspase-3 activation and ROS formation and increase tyrosinase activity and melanin level in MC induced by UVB (250, 62.5 and 125 mJ/cm², respectively). A431 cells failed to exert the apoptotic, oxidative stress and melanogenic response. In addition, CM from KC provided the highest modulatory effects against UVB-mediated MC responses.

3.4 The paracrine protective effects on UVB-induced genes encoding secreted paracrine factors in KC.

We next investigated the modulatory paracrine factors produced by KC and observed that UVB (125 mJ/cm²) irradiation caused an induction of paracrine factors (Corticotropin releasing hormone, CRH; CRHR1, corticotropin releasing hormone receptor 1; ET-1, endothelin-1; alphamelanocyte-stimulating hormone; POMC) mRNA expression at 6 h and 8 h post-irradiation in KC (Fig. 5A). Therefore 6 h after UVB (125 mJ/cm²) irradiation, selected cells including KC, HaCaT, HDF and A431 were collected to detamine paracrine factors responsible for the paracrine protective effects of KC using RT-PCR (Fig 5B). Our results revealed that, upon UVB (125 mJ/cm²) irradiation, increased levels of mRNA levels of 3 paracrine factors (CRHR1, ET-1 and POMC) in KC. In addition, the highest upregulation of ET-1 mRNA was found in KC irradiated with UVB (125 mJ/cm²). However, the mRNA expressions of 3 paracrine factors studied were not present in HDF and A431. In addition, increased ET-1 mRNA expression was also observed in HaCaT in response to UVB irradiation. Our results revealed that, ET-1 may be a possible candidate paracrine factors of KC that plays a crucial role in maintaining cellular homeostasis and cytoprotection against UVB-induced MC responses.

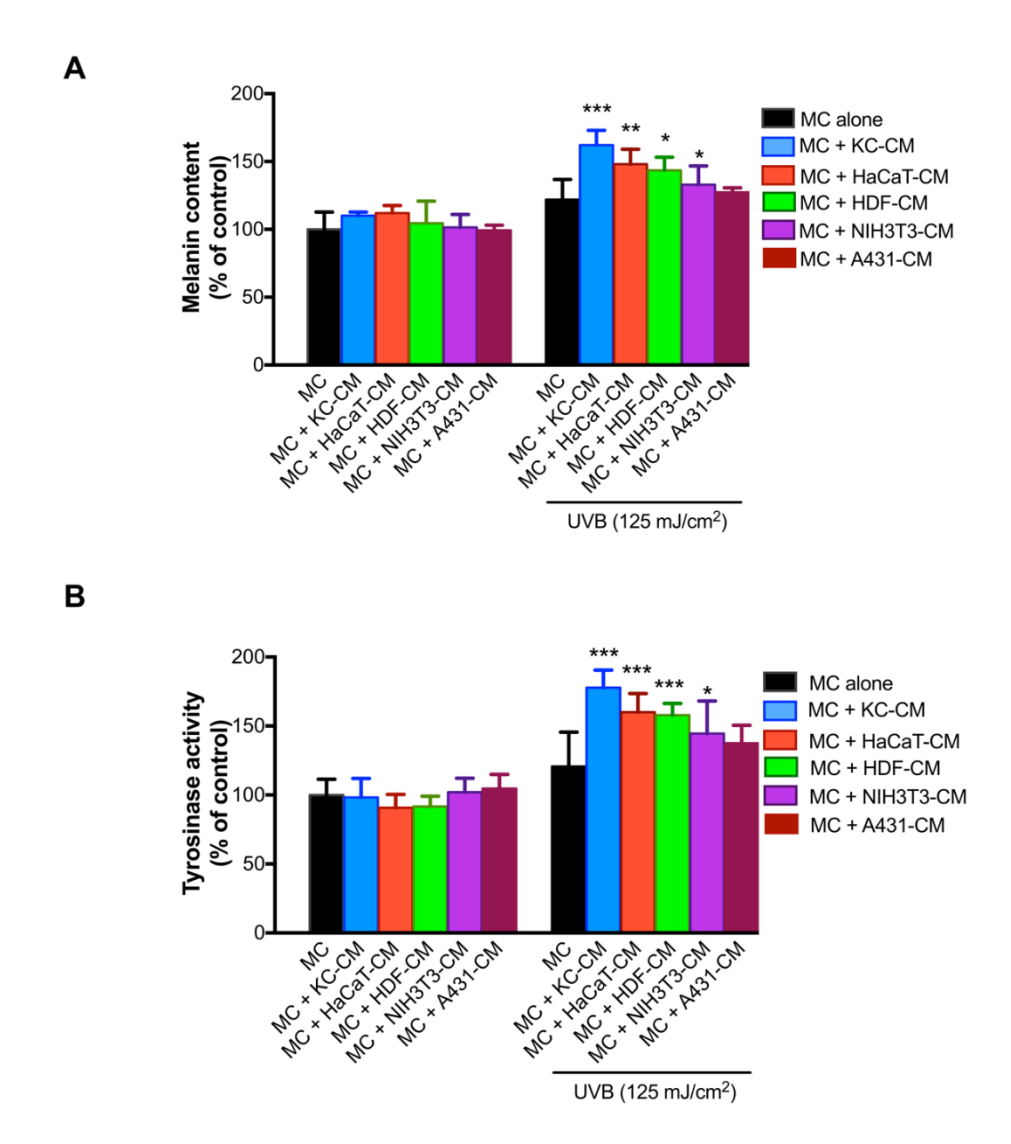


Fig 3. The protective effects of KC, HaCaT, HDF, NIHT3T, A431 cells on UVB-induced melanogenesis in MC treated with CM from KC, HaCaT, HDF, NIHT3T, A431 cells. The effects of UVB on melanin content (A) and tyrosinase activity (B) in MC pretreated with CM from KC, HaCaT, HDF, NIHT3T, A431 irradiated with UVB (125 mJ/cm²) for 30 min. The statistical significance of differences between UVB-irradiated MC and UVB-irradiated MC+KC-CM, MC+HaCaT-CM, MC+HDF-CM, MC+NIH3T3-CM and MC+A431-CM was evaluated by one-way ANOVA followed by Dunnett's test (*P < 0.05, **P < 0.01, ***P < 0.001 versus UVB-irradiated MC)

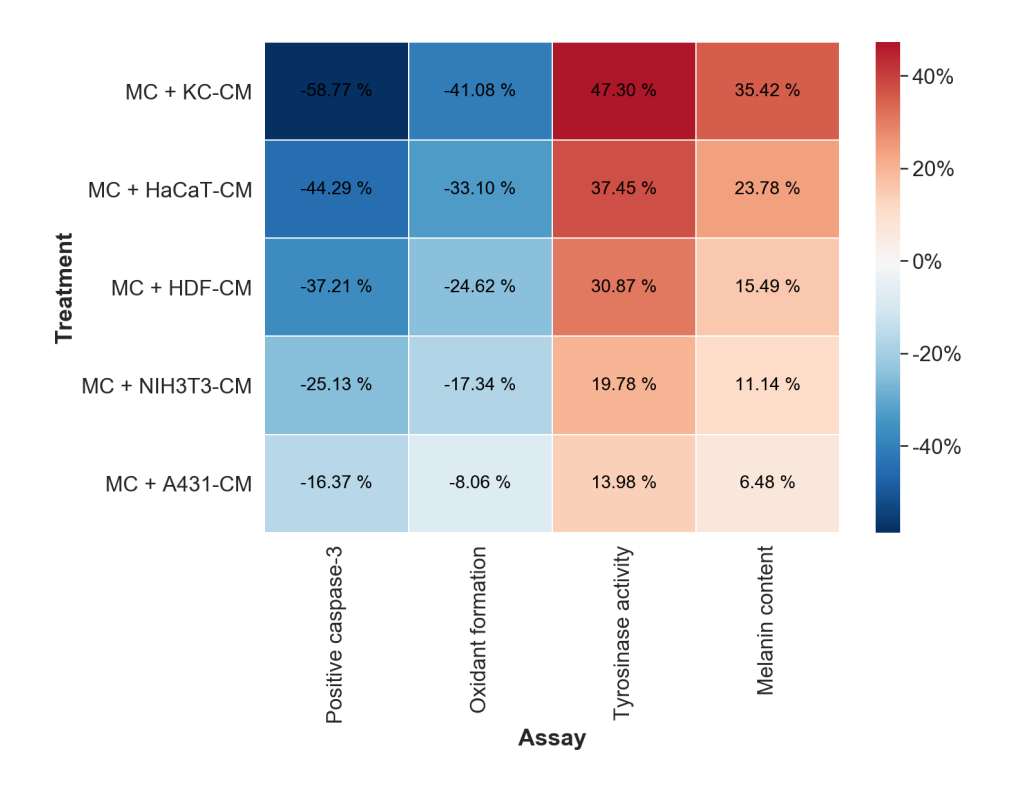
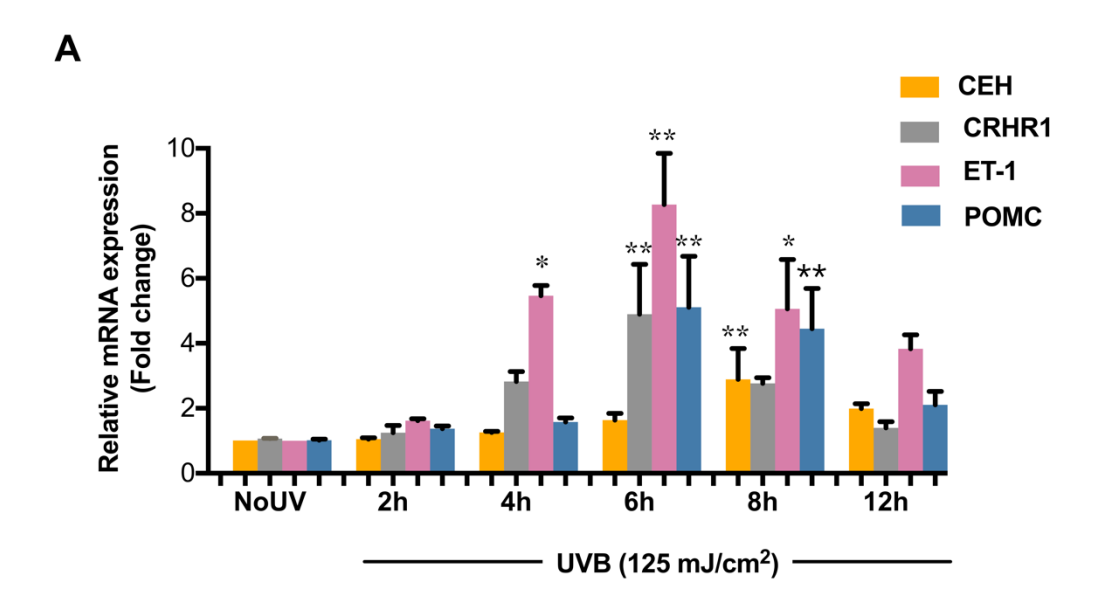


Fig 4. Heatmap analysis of the protective effects of KC, HaCaT, HDF, NIHT3T, A431 cells on UVB-induced apoptosis, oxidative stress and melanogenesis in MC treated with CM from KC, HaCaT, HDF, NIHT3T, A431 cells. Heat map representing color-coded expression levels of the paracrine protective effects of KC, HaCaT, HDF, NIHT3T, A431 cells on UVB-induced MC responses. The blue color represented the inhibitory action of paracrine protective effects. The red color represented the activating action of paracrine protective effects.



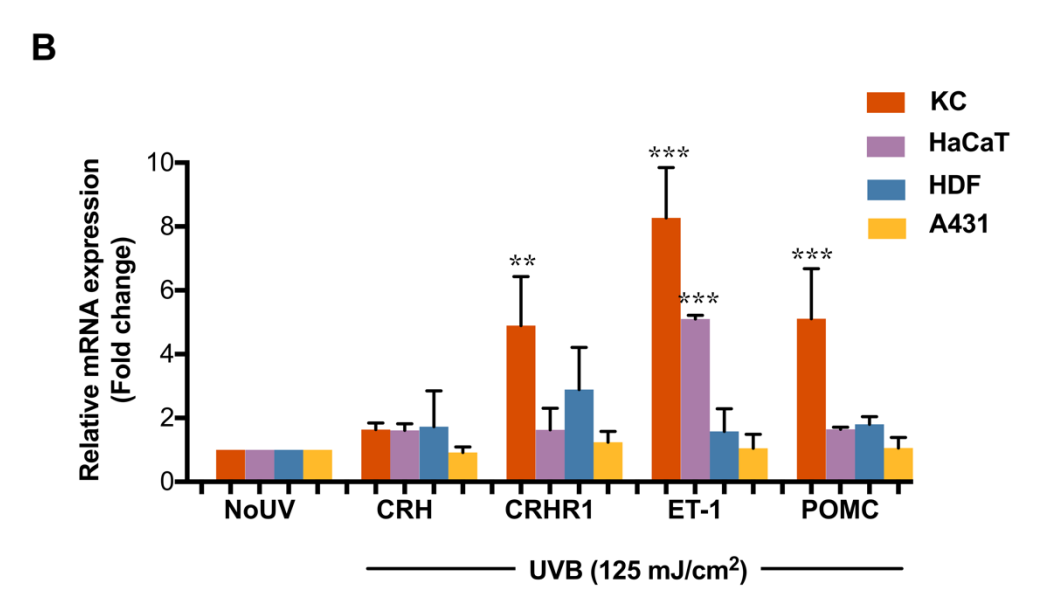
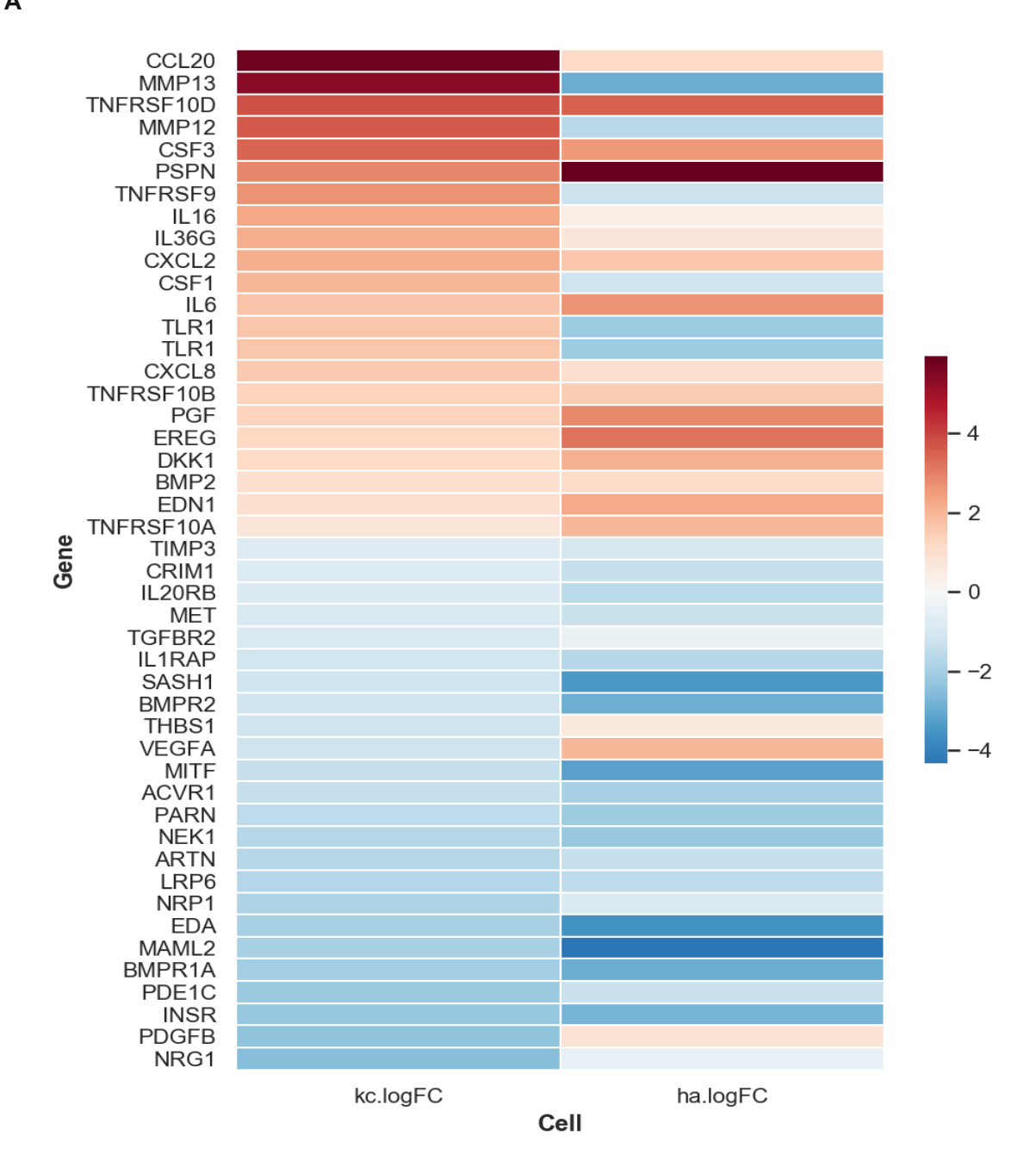
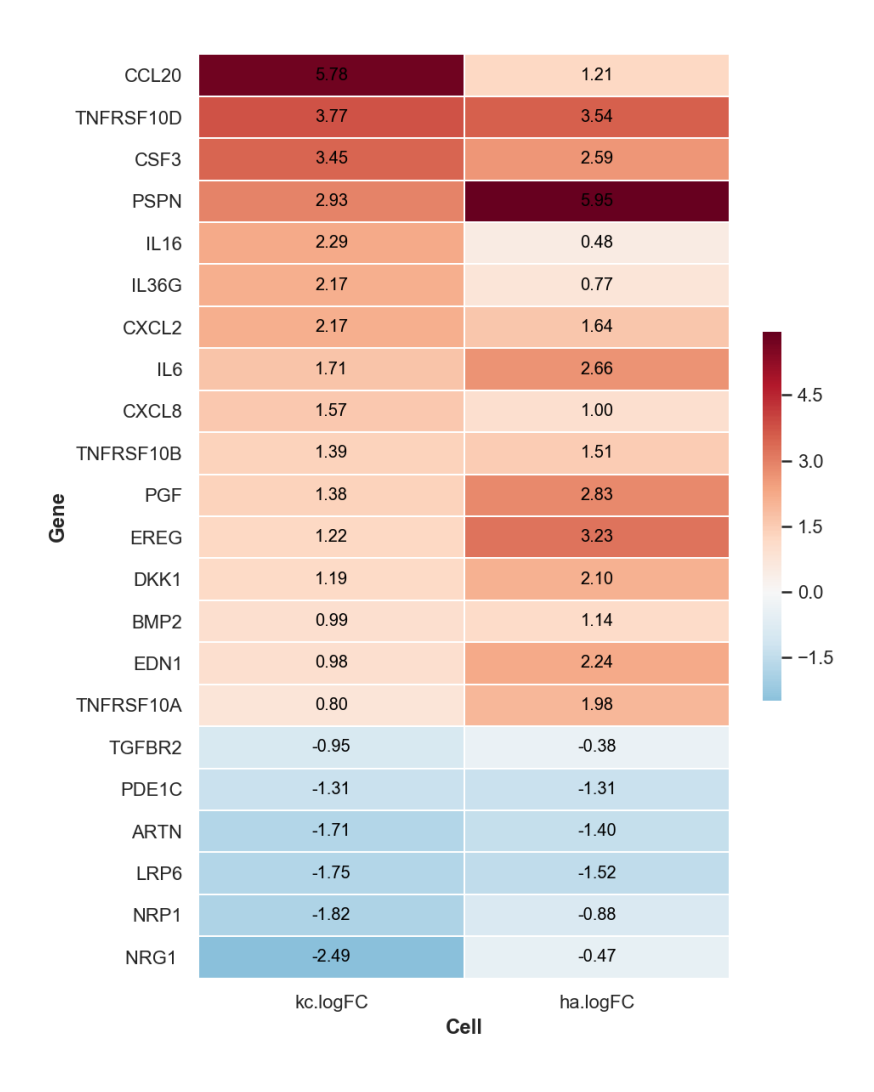


Fig 5. The effects of UVB on genes encoding secreted paracrine factors (CRH, CRH1, ET-1, POMC) expression in KC, HaCaT, HDF, A431 cells. Time-dependent effects of UVB (1250 mJ/cm^2) on CRH, CRH1, ET-1, POMC mRNA expression at 2, 4, 6, 8, 12 h post-irradiation in KC cells (A). The statistical significance of differences was evaluated by one-way ANOVA followed by Dunnett's test. *P < 0.05; **P < 0.01 versus unirradiated KC. The effects of UVB (250 mJ/cm^2) on mRNA levels of the paracrine factors (ET-1, CRH, CRHR1 and POMC) at 6 h post-irradiation in KC, HaCaT, HDF, A431 cells. The statistical significance of differences was evaluated by one-way ANOVA followed by Dunnett's test. **P < 0.01; ***P < 0.001 versus unirradiated cells.

3.5 Candidate genes encoding paracrine factors (PF) in KC and HaCaT responsible for their protective effects on UVB-mediated MC responses.

We next identified the candidate paracrine factors secreted by KC responsible for their protective effects on UVB-mediated MC responses. 6 h after UVB (125 mJ/cm²) irradiation, selected cells including KC and HaCaT were collected to determine paracrine factors responsible for the paracrine protective effects of KC using systems approach (RNA-seq). Differential gene expression (DEGs) was done using BioJupies platform. DEGs were identified by comparing the gene expression profile of UVB treated cells to the expression profile of the control cells. The DEGs profile indicated that all of the expressed genes were up-regulated, and downregulated as induced by the treatment of KC and HaCat cells with UVB radiation (125 mJ/cm2). The result indicated that a total of 1730 genes were identified as being differentially expressed (FDR≤0.05) between UVB (125 mJ/cm²) treated KC, HaCaT and control cells. Moreover, using paracrine factor gene list from database to define the genes encoding paracrine factors from 1730 genes. The results showed that UVB treated KC and HaCaT cells caused a significant expression of 48 paracrine factor genes compared to unirradiated cells (Fig 6A). This UVB (125 mJ/cm²) treatment produced 16 up-regulated transcripts in both KC and HaCaT (Fig 6B). To address whether KC provided the highest modulatory effects against UVB-mediated MC responses, we observed that 7 paracrine factor genes including CCL20, TNFRSF10D, GCSF, IL6, IL36G, CXCL2, CXCL8 were significantly upregulated in UVB- treated KC greater than UVB-teated HaCaT cells (Fig 6C). In addition, investigate the role of the candidate paracrine factors in UVB-induced oxidative stress, apoptosis and melanogenesis in MC treated candidate paracrine factor ligands should be performed to identify possible paracrine factors responsible for the modulatory paracrine effects of KC.





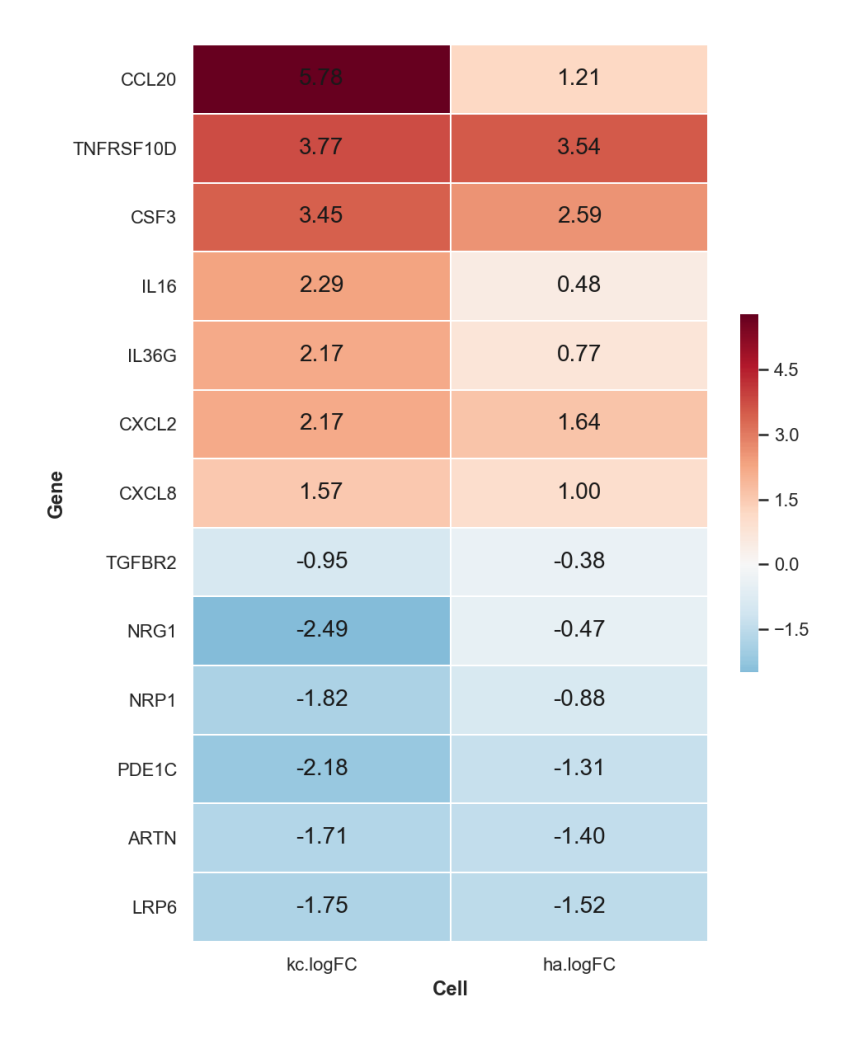
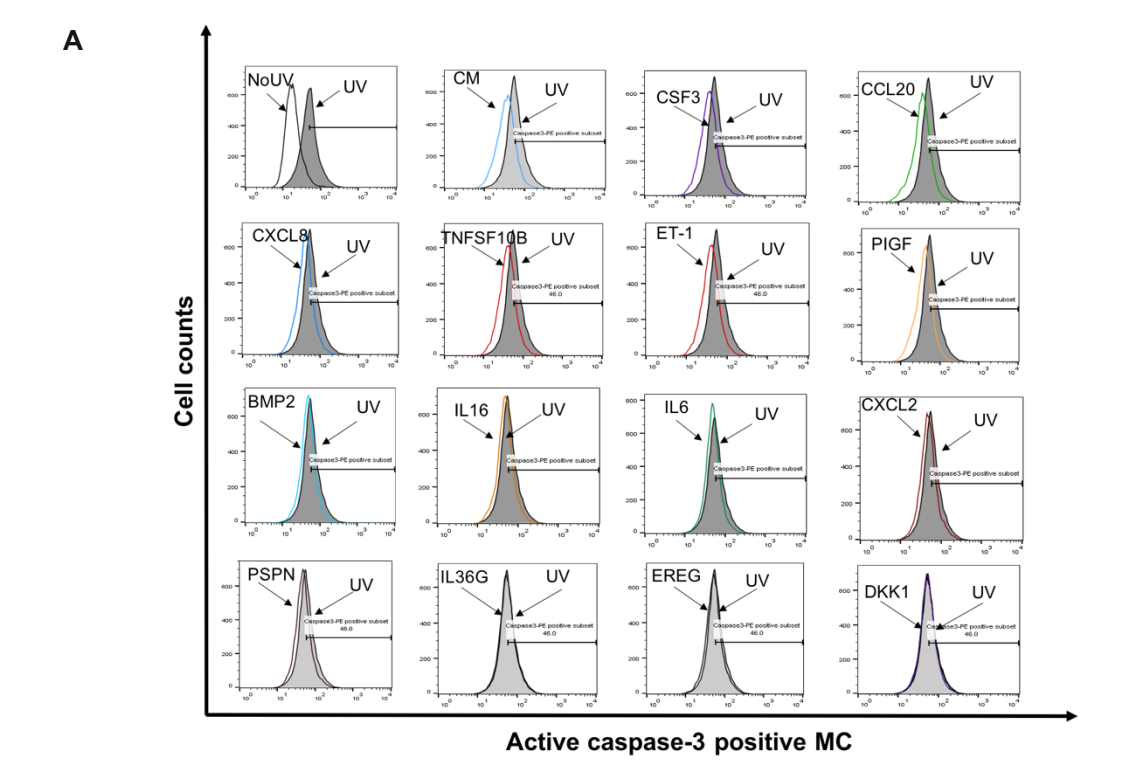
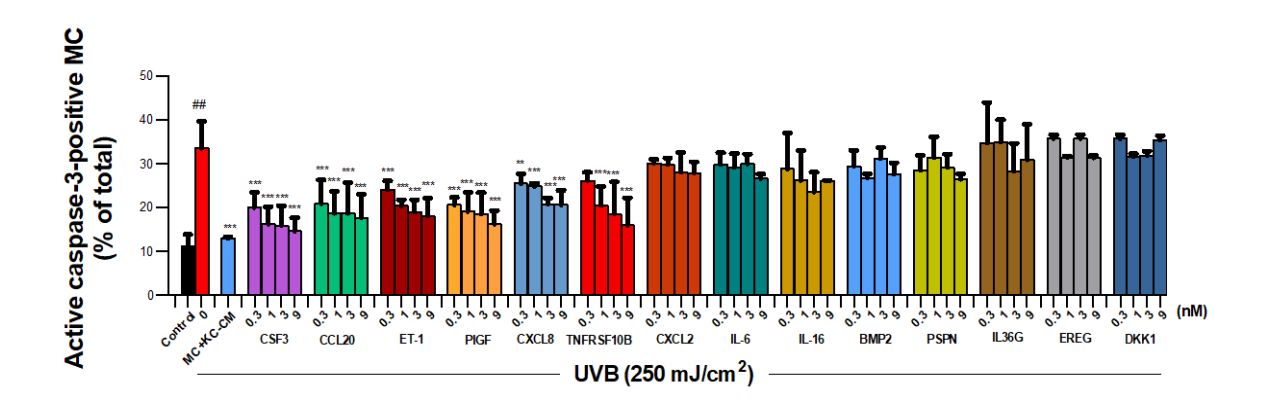


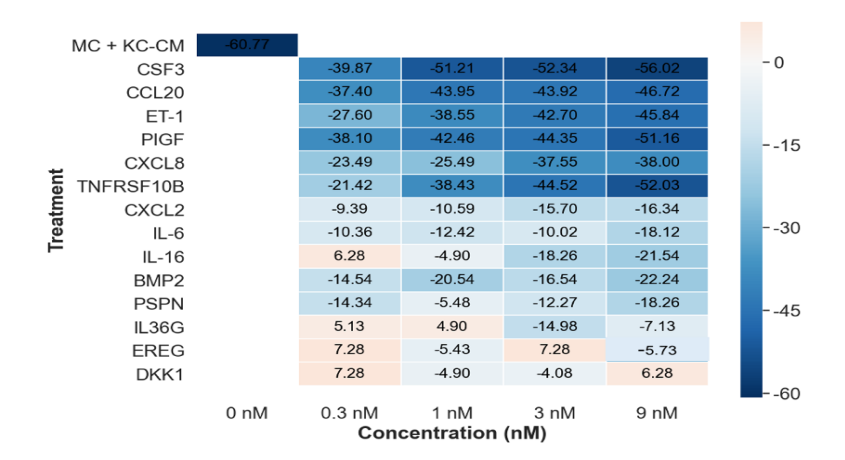
Fig 6. The effects of UVB on genes encoding secreted paracrine factors expression in KC and HaCaT cells. Heatmap analysis of differentially expressed genes of UVB irradiated keratinocytes (KC) and HaCaT (ha) cells. The data were presented on a log2 fold change of UVB-irradiated cells versus unirradiated cells (control cells). Red color represents up-regulated genes, blue color represents non-differentially expressed genes. A total of 1730 genes were identified as being differentially expressed (FDR≤0.05) between UVB treated and control cells (A). UVB (125 mJ/cm²) treatment caused 16 up-regulated transcripts in both KC and HaCaT (B). 7 paracrine factor genes were significantly upregulated in UVB-treated KC more than UVB-treated HaCaT cells.

3.6 The protective effects of paracrine factors on UVB (250 mJ/cm²)-induced apoptosis in MC cells.

To confirm that the identified paracrine factors influenced cellular responses of MC to UVB, we evaluated the effects of recombinant paracrine factors on UVB-induced apoptosis (Fig. 7A) ,melanogenesis (Fig 8A) and ROS formation (Fig 9) in MC Then, we highlighted the 14 candidate genes including CSF3 or GCSF, CCL20, ET-1, PIGF, CXCL8, TNFRSF10B, CXCL2, IL-6, IL-16, BMP2, PSPN, IL36G, EREG, DKK1 and verified their functions in mitigating UVB-mediated stress responses of MC using recombinant paracrine factors. Among 14 recombinant proteins, 6 ligands including GCSF, CCL20, ET-1, PIGF, CXCL8, TNFRSF10B were observed to suppress caspase-3 activation, 5 ligands including GCSF, CCL20, ET1, PIGF, CXCL8 can stimulate melanin content in UVB-irradiated MC and 6 ligands including GCSF, CCL20, ET-1, CXCL8, TNFRSF10B, BMP2 were observed to suppress ROS formation. We also explored heatmap analysis to conclude the protective effects of paracrine factors on UVB-induced apoptosis and melanogenesis in MC (Fig 7B and 8B). The result showed that 4 ligands including GCSF, CCL20, ET-1, CXCL8 were observed to suppress caspase-3 activation, stimulate melanin content and inhibit ROS formation in UVB-irradiated MC, suggesting a correlation between the rescue activity of candidate paracrine and their corresponding transcripts expressed in KC. Then, GCSF and CCL20 providing the strongest modulatory effects on the MC responses were then chosen and verified as candidate paracrine factors responsible for the protective effects of KC on the damage response of MC to UVB. We next investigated the UVBinduced GCSF levels produced by KC (Fig 10). At 12 h post-irradiation, CM from KC at three cell concentrations (7x10³, 21x10³, 63x10³ cells/cm²) were collected and then GCSF concentrations were measured. The results observed that exposure of KC to UVB (125 mJ/cm²) led to a substantial increase in secretion of GCSF at all three different concentrations of KC, corresponding to the concentrations of the recombinant proteins having the biological effects on MC.

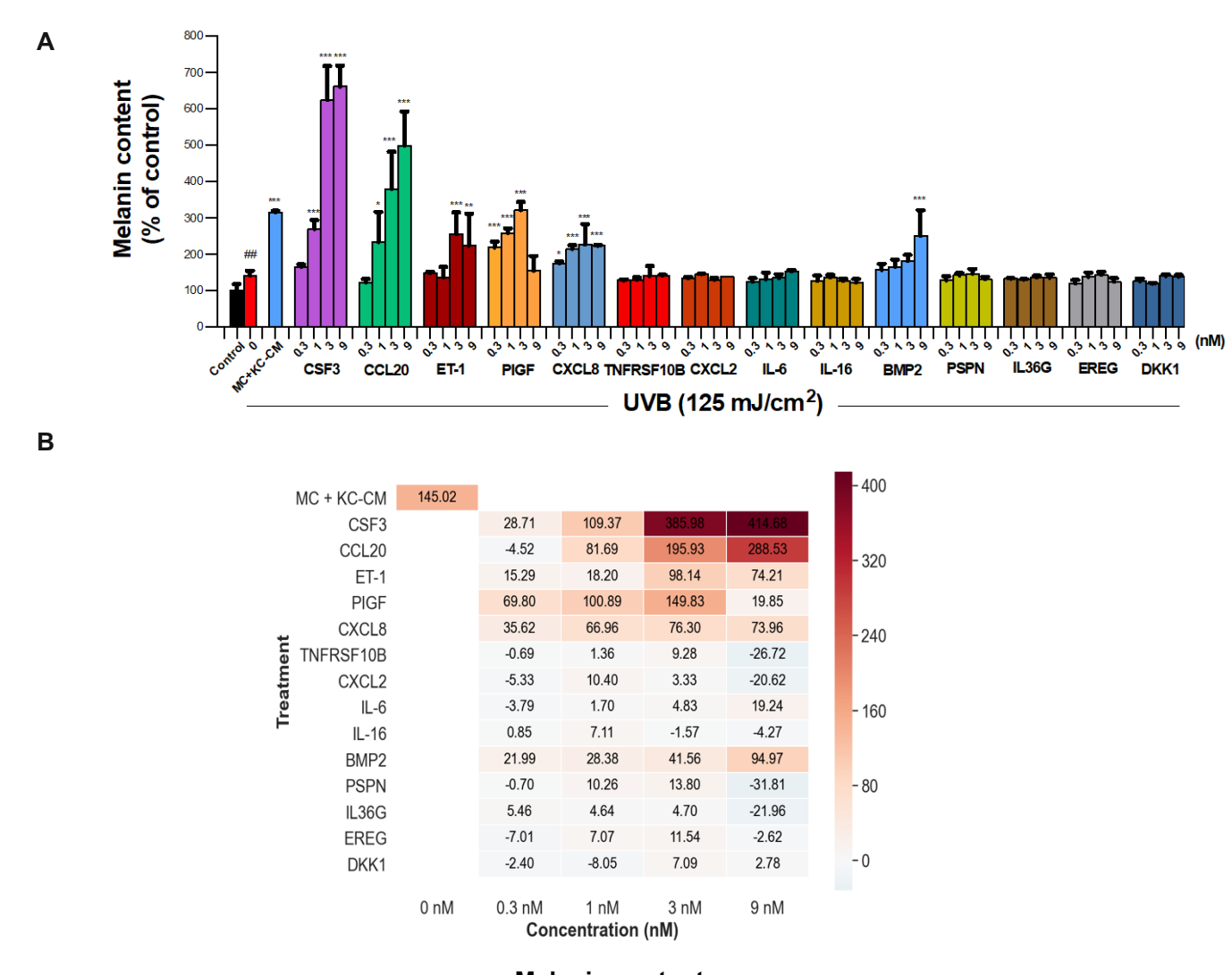






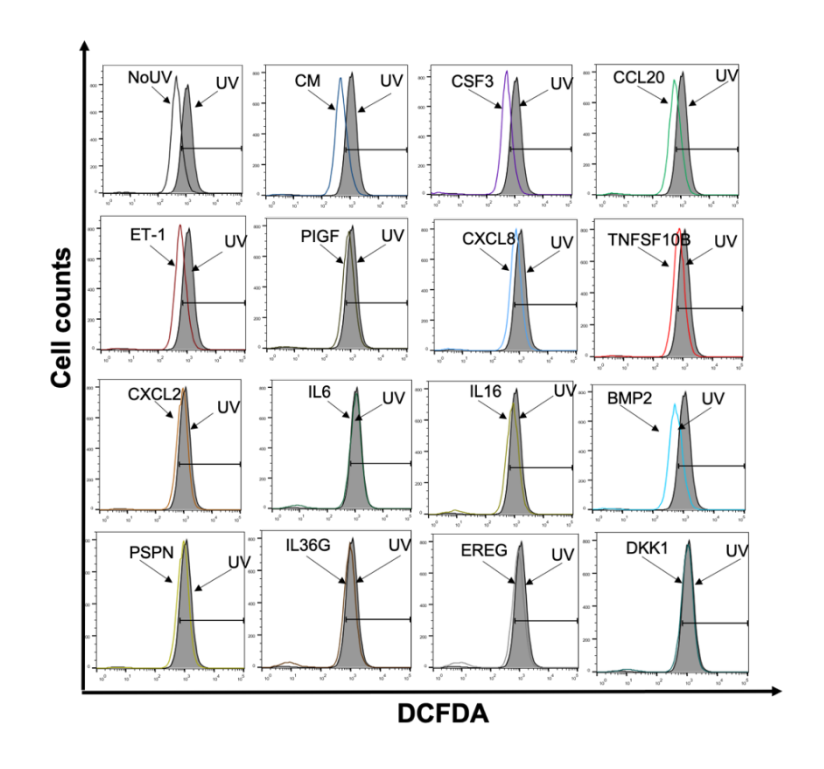
Caspase-3 activation

Fig 7. The protective effects of paracrine factors on UVB (250 mJ/cm²)-induced apoptosis in MC cells. (A) The effects of UVB on caspase3 activation in MC pretreated with CM from KC, irradiated with UVB (125 mJ/cm²) and 14 recombinant paracrine factors including GCSF, CCL20, ET-1, PIGF, CXCL8, TNFRSF10B, CXCL2, IL-6, IL-16, BMP2, PSPN, IL36G, EREG and DKK1 at concentrations of 0.3, 1, 3, and 9 nM. MC were harvested at 12 h after UVB irradiation for determination of active caspase-3 staining. Data was expressed as mean \pm SD. The statistical significance of differences between UVB-irradiated MC and UVB-irradiated MC+KC-CM, and 14 recombinant paracrine factors was evaluated by one-way ANOVA followed by Dunnett's test (*P < 0.0; *P < 0.01; ***P < 0.001 versus UVB-irradiated MC). (B) Heat map representing color-coded expression levels of the paracrine protective effects of KC and 14 recombinant paracrine factors on UVB-induced apoptosis in MC cells. The blue color represented the inhibitory action of paracrine protective effects.



Melanin content

Fig 8. The protective effects of paracrine factors on UVB (125 mJ/cm²)-induced melanin content in MC cells. (A) The effects of UVB on melanin content in MC pretreated with CM from KC, irradiated with UVB (125 mJ/cm²) and 14 recombinant paracrine factors including GCSF, CCL20, ET-1, PIGF, CXCL8, TNFRSF10B, CXCL2, IL-6, IL-16, BMP2, PSPN, IL36G, EREG and DKK1 at concentrations of 0.3, 1, 3, and 9 nM for 2 h. MC were harvested at 12 h after UVB irradiation for determination of melanin content. Data was expressed as mean \pm SD. The statistical significance of differences between UVB-irradiated MC and UVB-irradiated MC+KC-CM, and 14 recombinant paracrine factors was evaluated by one-way ANOVA followed by Dunnett's test (*P < 0.05; *P < 0.01; ***P < 0.001 versus UVB-irradiated MC). (B) Heat map representing color-coded expression levels of the paracrine protective effects of KC and 14 recombinant paracrine factors on UVB-induced melanogenesis in MC cells. The blue color represented the inhibitory action of paracrine protective effects.



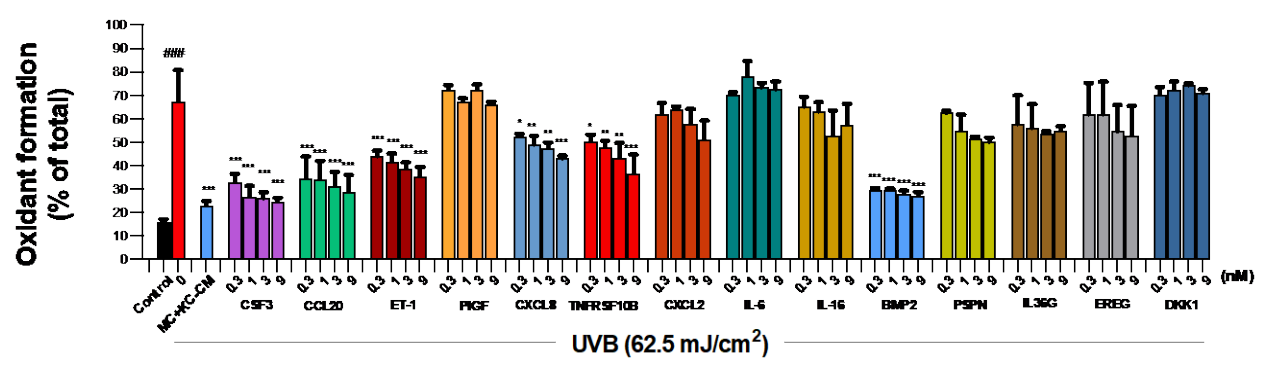


Fig 9. The protective effects of paracrine factors on UVB (62.5 mJ/cm 2)-induced ROS formation in MC cells. The effects of UVB on ROS formation in MC pretreated with KC-CM and 14 recombinant paracrine factors including GCSF, CCL20, ET-1, PIGF, CXCL8, TNFRSF10B, CXCL2, IL-6, IL-16, BMP2, PSPN, IL36G, EREG and DKK1 (0.3, 1, 3, and 9 nM) for 2 h. Data was expressed as mean \pm SD. The statistical significance of differences between UVB-irradiated MC and UVB-irradiated MC+KC-CM, and 14 recombinant paracrine factors was evaluated by one-way ANOVA followed by Dunnett's test (*P < 0.05; ***P < 0.001 versus UVB-irradiated MC).

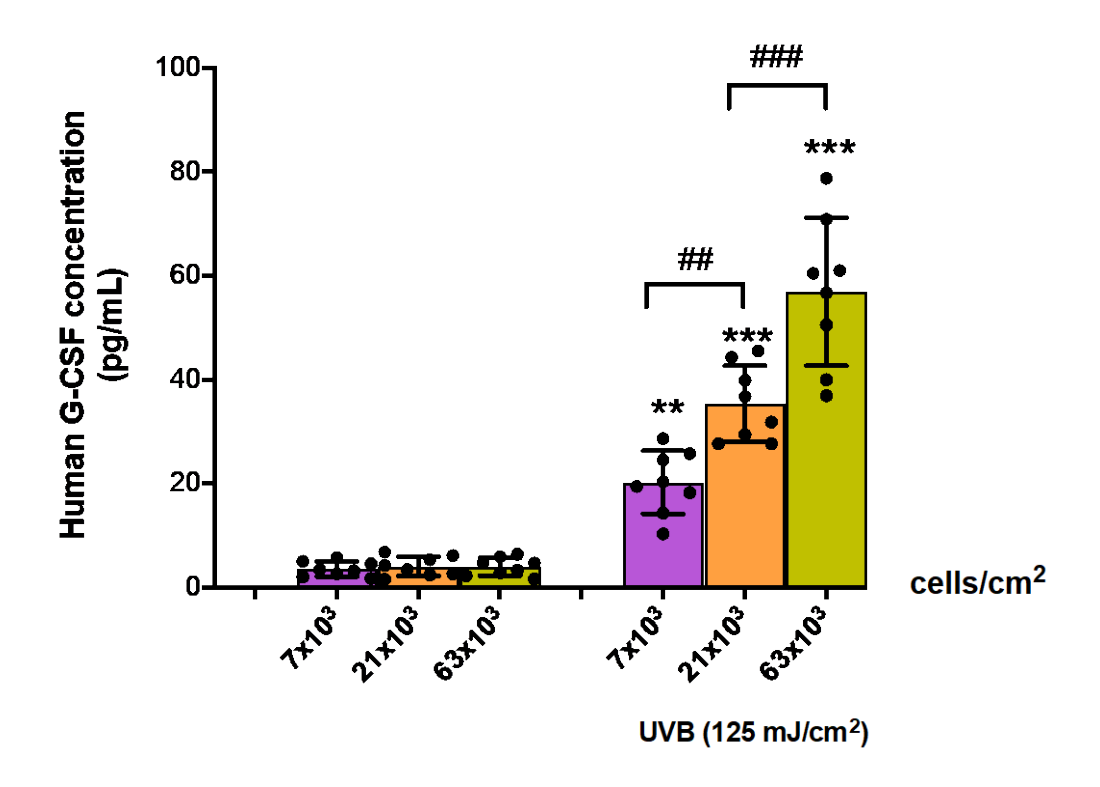


Fig 10. The effects of UVB (125 mJ/cm²) on GCSF levels in KC cells.

At 12 h post-irradiation, CM from KC at three cell concentrations $(7x10^3, 21x10^3, 63x10^3 \text{ cells/cm}^2)$ were collected and then GCSF concentrations were measured. Data was expressed as mean \pm SD. The statistical significance of differences between UVB-irradiated KC at different cell concentrations $(7x10^3, 21x10^3, 63x10^3 \text{ cells/cm}^2\text{at cell ratios})$ was evaluated by one-way ANOVA followed by Dunnett's test ((**P < 0.01; ***P < 0.001 versus unirradiated control KC). ## P < 0.01; ### P < 0.001versus UVB-irradiated KC at cell concentrations (7x10³ and 21x10³)

3.7 The protective effects of paracrine factors on UVB-induced melanogenesis in mouse skin exposed to UVB irradiation.

Since transcriptional profiling of KC in the skin can be influenced by the surrounding non-KC cell types, we then employed a mouse model of UVB-induced photodamage which could represent a physiologically relevant approach to demonstrate the *in vivo* relevance of the *in vitro* findings. Immunofluorescence analysis revealed a correlation between expression of GCSF and CCL20 proteins in epidermis and the major melanogenic enzyme tyrosinase, an indicative of the MC responses, in mouse skin exposed to UVB irradiation (500 - 1,000 mJ/cm²). Immunofluorescent stained sections of skin tissues revealed that UVB (500 - 1,000 mJ/cm²) treatment markedly increased GCSF and CCL20 expression (Figure 11A, B, C and D) as well as tyrosinase expression (Figures 11A, B and E). Therefore, there is a correlation of increased expression of paracrine proteins, GCSF and CCL20, and tyrosinase, the enzyme responsible for melanin synthesis. In summary, our study demonstrated that the GCSF and CCL20 may be candidate paracrine factors secreted from KC that contribute to a regulatory role on the stress responses of MC to UVB.

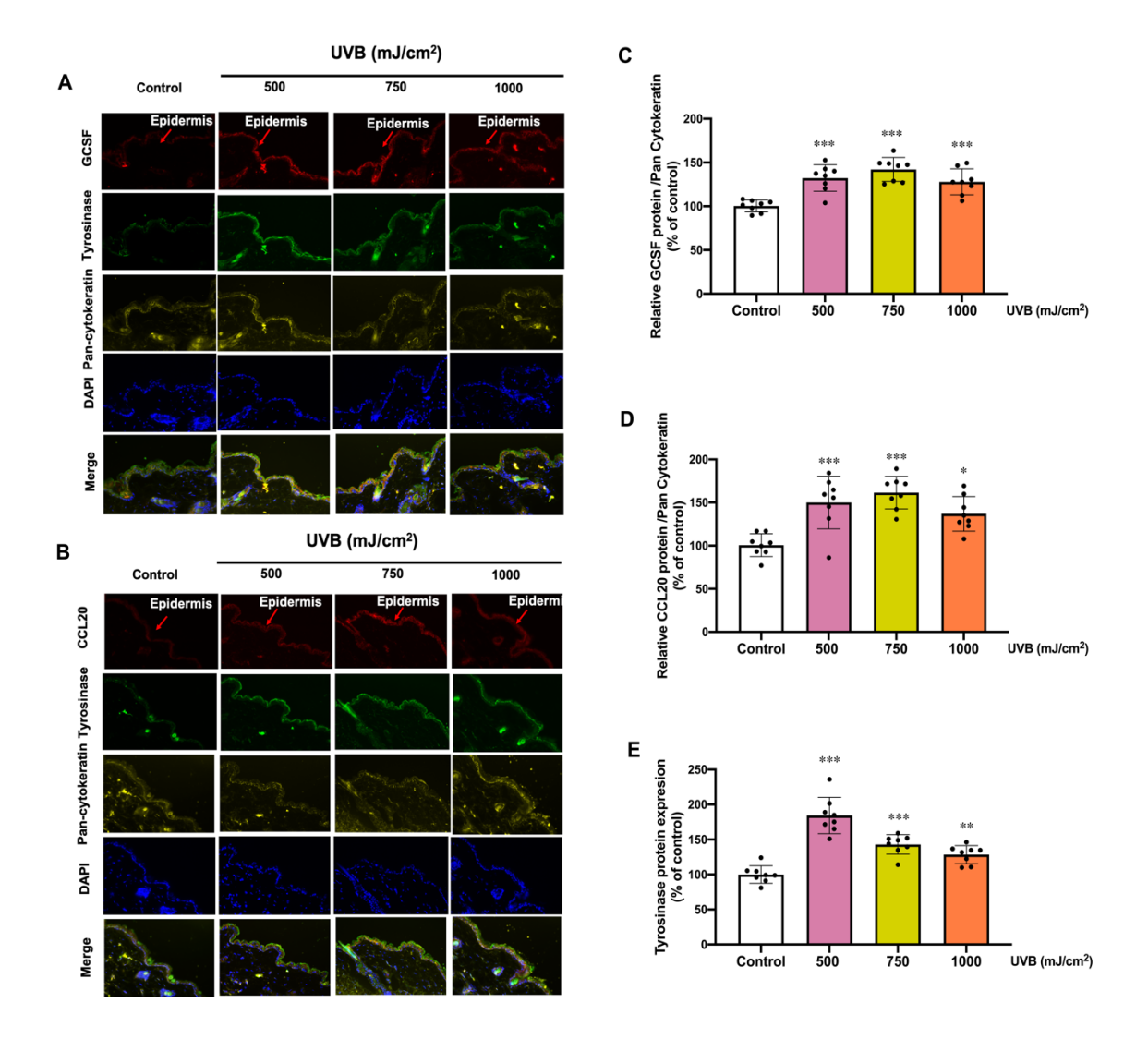


Fig 11. The expression of GCSF, CCL20 and tyrosinase protein in mouse skin exposed to UVB irradiation. The immunofluorescence of GCSF (A), CCL20 (B), Tyrosinase (A and B) and pancytokeratin which is keratinocyte marker (A and B) were collected at 12 h following the final UVB exposure. The summary graph with the statistical analysis of the relative protein levels of GCSF (C), CCL20 (D) to pan-cytokeratin and tyrosinase (F) were quantified by ImageJ and graphpad prism software and were expressed as mean \pm SD, 1 N (dot) = one area from 4 areas in a mouse. A mouse provides 4 N. * P < 0.05, **P < 0.01, ***P < 0.001 versus non-irradiated group, one-way ANOVA with post-hoc Dunnett's test.

Part II. *In vivo* study on the anti-photoaging effects of mitochondria-targeted molecules, herbal extracts (Harak formula), Nrf2 inducers and topical-based nanoparticles incorporated with medicinal plants (Harak formula) and its bioactive.

3.8 HRF and HSP protected against UVA-induced skin damage in BALB/c mice in vivo

To establish the *in vivo* mouse model of skin photoaging, we tested the anti-photoaging effects of potential herbal formula HRF and its possible active ingredient HSP observed to show the antioxidant and anti-aging properties in NHDFs irradiated with UVA. This study then examined the effects of the HRF and HSP on UVA-induced photoaging in a relevant *in vivo* mouse model. The HRF and HSP were topically applied to the mouse dorsal skin for 1 h prior to UVA irradiation (total cumulative dose 60 J/cm²). H&E and IF staining of skin tissue sections revealed that UVA treatment markedly induced epidermal thickness (Fig. 12A and D) and MMP-1 protein expression (Fig. 12B and E) as well as reduced collagen type 1 protein levels (Figure 12C and F). In contrast, the topical treatment of mouse skin with HRF (10-100 mg/cm²) and HPS (0.3-3 mg/cm²) led to the reduction of the epidermal thickness (Fig. 12A and D) and MMP-1 protein expression (Fig. 12B and E) as well as the induction of collagen type 1 protein levels (Fig. 12C and F). As expected, positive control, sulforaphane (SFN) also provided these protective effects (Fig. 12A-F).

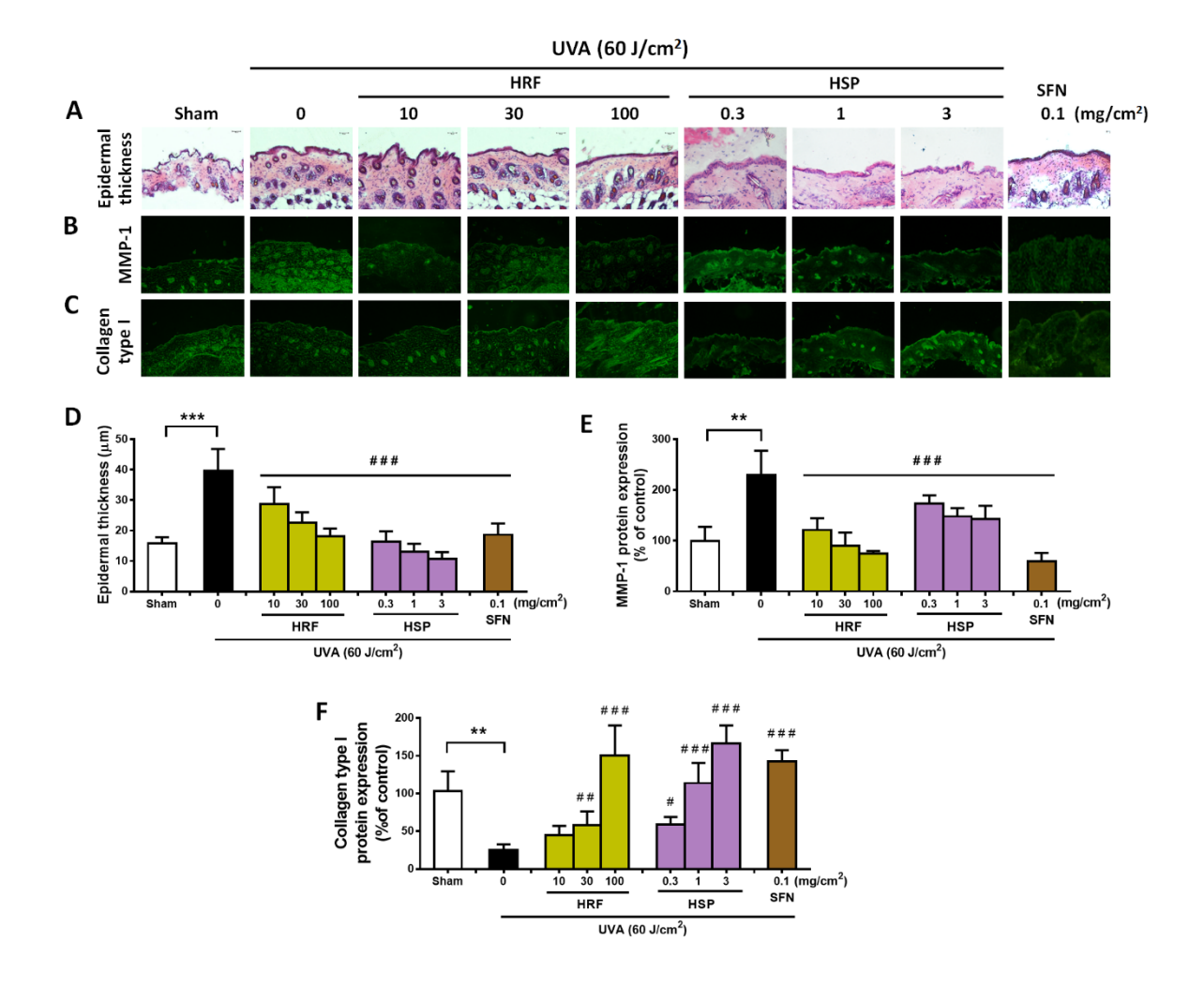


Fig. 12. The protective effects of HRF and HSP on UVA-induced skin damage in the in vivo model.

BALB/c mice were topically applied with 10, 30, and 100 mg/cm² HRF and 0.3, 1, and 3 mg/cm² HSP as well as the ethanol treatment and no compound treatment (0) on the dorsal skin for 1 h prior to each UVA irradiation (10 J/cm²/session 3 times a week for 2 weeks; a cumulative total dose of 60 J/cm²). Images of H&E staining for epidermal thickness (A) and the immunofluorescence of MMP-1 (B) and collagen (C) were collected at 24 h following the last UVA exposure. The summary graph with the statistical analysis of epidermal thickness (D) and the protein levels of MMP-1 (E) and collagen (F) was quantified by ImageJ and GraphPad Prism software. Data was shown as mean \pm SD at the 20X magnification (scale bar = 50 μ m), n = 4. **P < 0.01, ***P < 0.001 versus non-irradiated sham group by Student's t-test. # P < 0.05; ## P < 0.01; ### P < 0.001 versus the sham-irradiated group by one-way ANOVA Dunnett's test.

3.9 HRF and HSP suppressed downregulation of Nrf2 levels and its downstream signaling in UVA-induced photodamage of mouse skin *in vivo*

Since Nrf2 is required for protection against UVA-stimulated MMP-1 upregulation, we thus further examined whether HRF and HSP could protect against the skin photoaging through this pathway in mouse skin *in vivo*. At 1 h post-irradiation, the nuclear Nrf2 levels were significantly reduced in the mouse skin exposed to the UVA irradiation (60 J/cm²) (Fig. 13A) and this reduction was dose-dependently inhibited by HRF and HSP (30-100 mg/cm² and 3 mg/cm²) (Fig. 13E). The HRF (30-100 mg/cm²) and HSP (3 mg/cm²) also markedly abrogated UVA-induced reduction of GST protein levels (Fig. 13B and F). The decline of NQO-1 protein levels was also significantly inhibited by HRF and HSP in a concentration-dependent manner (10-100 mg/cm² and 0.3-3 mg/cm²) in mouse skin exposed to UVA (Fig. 13C and G). To evaluate the photoprotective effect of HRF and HSP on UVA-mediated oxidative DNA damage, the formation of 8-hydroxy-2′-deoxyguanosine (8-OHdG), a sensitive marker of oxidative DNA damage, was quantified in the mouse dermis at 1 h following the final UVA exposure with cumulative doses of 60 J/cm². The results indicated that UVA irradiation increased the skin levels of 8-OHdG indicative of inducing oxidative DNA damage. However, HRF (30-100 mg/cm²) and HSP (0.3-3 mg/cm²) dose-dependently protected against UVA-induced oxidative DNA damage in the mouse skin (Fig. 13D and H).

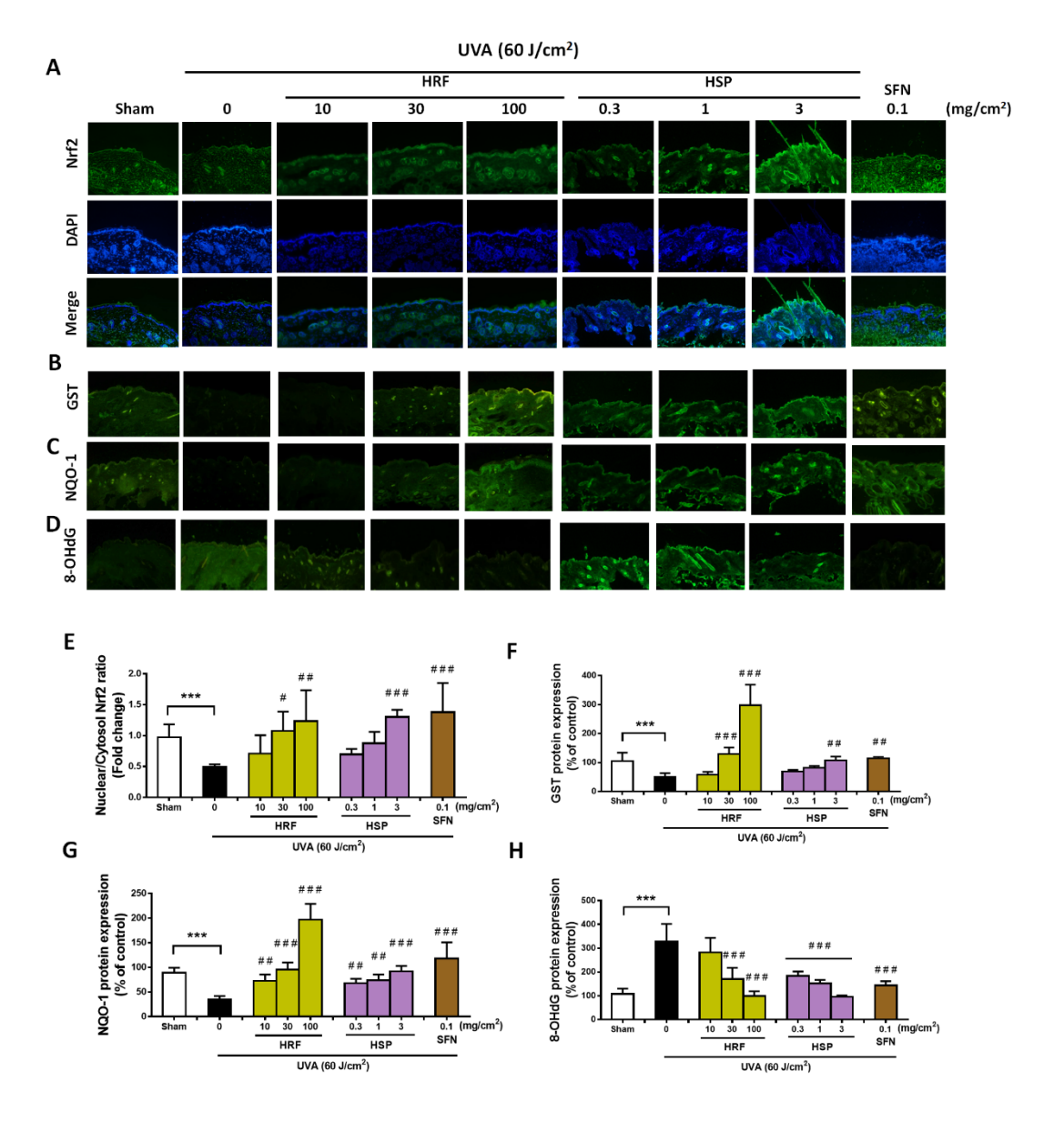


Fig. 13. The modulation of the Nrf2-mediated antioxidant response by HRF and HSP in mouse dorsal skin irradiated with UVA. Images of immunofluorescence staining (FITC-conjugated secondary antibody staining indicated the location of Nrf2 (green by the anti-Nrf2 antibody. DAPI staining indicated the location of the nucleus (blue) and the merged image indicated the nuclear localization of Nrf2 (A). The summary graph with the statistical analysis of the nuclear-to-cytosolic Nrf2 ratio (E) was quantified by ImageJ and GraphPad prism software and was expressed as mean \pm SD, n = 4. The immunofluorescence of antioxidant proteins including GST (B), NQO-1 (C), and the oxidative DNA damage 8-OHdG (D), were collected at 6 h following the final UVA exposure. The summary graph with the statistical analysis of the protein levels of GST (F), NQO-1 (G), and 8-OHdG (H) were quantified by ImageJ and GraphPad prism software and were expressed as mean \pm SD, n = 4. ***P < 0.001 versus non-irradiated sham group by Student's t-test. #P < 0.05; ##P < 0.01; ###P < 0.001 versus the shamirradiated group by one-way ANOVA Dunnett's test.

3.10 Effects of mitochondrial-targeted molecules (AP39 and AP123) against UVA-induced skin damage in BALB/c mice *in vivo*

We previously showed UVA irradiation of mouse skin caused a dose-dependent upregulation of MMP-1 expression, collagen I degradation and increased epidermal thickness at 24 h after the final irradiation (10 J/cm², cumulative dose, 60 J/cm²). We therefore used this model for our studies with AP39 and AP123, and controls. Compounds (0.3 and 0.1 μ M/cm²) were applied topically to dorsal mouse skin for 1 h and then irradiated with UVA (total dose 60 J/cm²). UVA treatment markedly reduced epidermal thickness (Fig. 14A and D) and increased MMP-1 (Fig. 14B and E) and collagen levels (Fig. 14C and F), and this effect was not attenuated by non-targeted H₂S (1 μ M/cm², ADT-OH or HTB). However, AP39 and AP123 (0.3 and 1 μ M/cm²) decreased epidermal thickness (Fig. 14A and D), inhibited MMP-1 activation (Fig. 14B and E) and increased collagen-1 levels (Fig. 14C and F). These protective effects were also observed with the positive control, Nrf2 activator sulforaphane (SFN; Fig. 14A-F).

3.11 AP39 and AP123 activated Nrf2-regulated redox signaling in mouse skin in vivo

Figures 15A and F show UVA exposure (60 J/cm 2) lowered nuclear Nrf2 levels in mouse skin, and this decline was dose-dependently inhibited by AP39 and AP123 (0.1-0.3 μ M/cm 2) but not by non-targeted controls (ADT-OH and HTB respectively. Additionally, AP39 and AP123 (but not controls) significantly dose-dependently inhibited UVA-induced decline in glutamate-cysteine ligase (GCLC) glutathione-S-transferase (GST) and NQO-1 levels (Fig. 15G-I, respectively) as well as prevented oxidative DNA damage (8-OHdG; Fig. 15E and J. positive control also attenuated these parameters, as expected (Fig. 15).

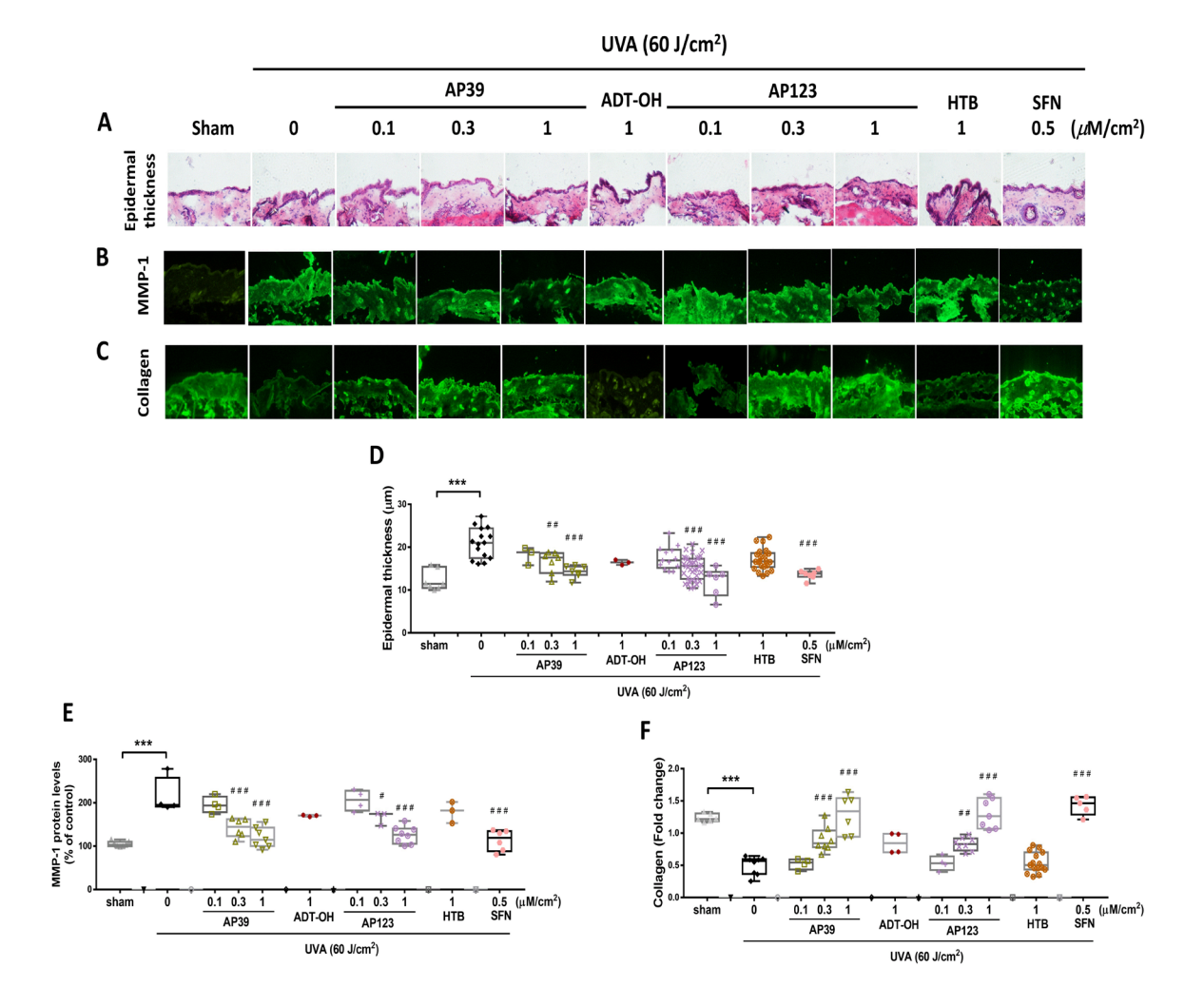


Fig. 14 Topical application of mitochondria-targeted molecules (AP39 and AP123) prevented UVA-induced skin damage in BALB/c mice. AP39 and AP123 (0.1, 0.3 and 1 μ M/cm²), controls (1 μ M/cm²) or SFN (0.5 μ M/cm²) were applied to dorsal skin for 1 h prior to each UVA irradiation (10 J/cm²/session 3 times a week for 2 weeks; a cumulative total dose of 60 J/cm²). (A) Epidermal thickness by H&E staining. (B) MMP-1 and (C) collagen levels by immunofluorescence. (D-E) densitometric analysis (ImageJ) of epidermal thickness, MMP-1 and collagen levels, respectively. Data are mean ± SD at the 20X magnification (scale bar = 50 μ m), n = 4. ***P < 0.001 c.f. non-irradiated sham group Student's t-test. # P < 0.05; ## P < 0.01; ### P < 0.001 c.f. the sham-irradiated group, one-way ANOVA with post-hoc Dunnett's test.

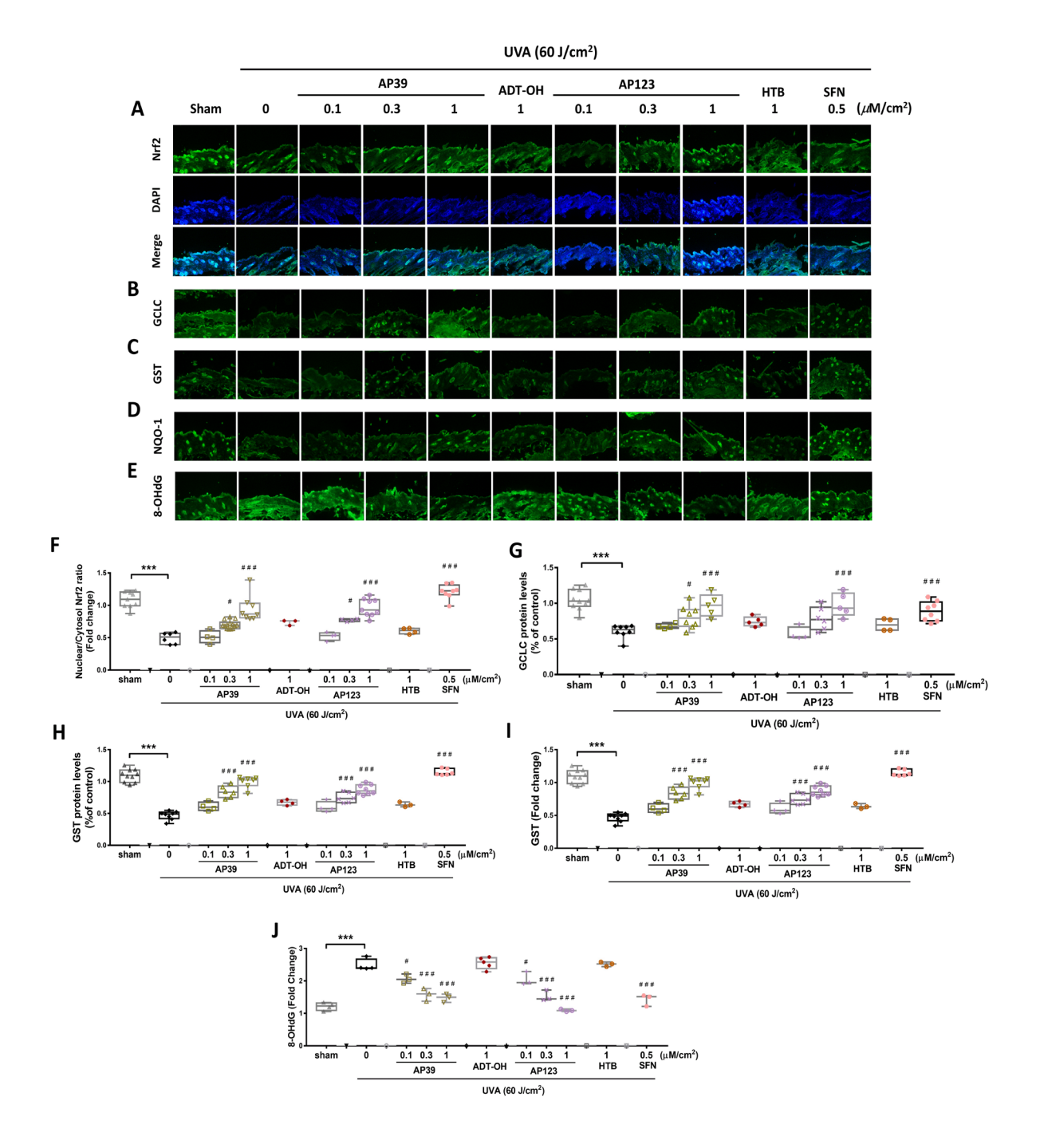


Figure 15. AP39 and AP123 promoted Nrf2-regulated redox signaling pathway in BABL/c mice irradiated with UVA. (A) Nrf2 immunofluorescence with DAPI nuclear counterstain and merged images. (B) GCLC (C) GST, (D) NQO-1 and (E) 8-OHdG expression in skin by immunofluorescence. (F-J) ImageJ quantification of (F) nuclear Nrf2 (G) GCLC, (H) GST, (I) NQO-1 and (J) 8-OHdG levels. Data shown are mean \pm s.d. of (n=4) *P < 0.05; **P < 0.01; *** P < 0.001 c.f. the sham-irradiation; #P < 0.05; ## P < 0.01; ### P < 0.001 c.f. UVA treatment, one-way ANOVA with post-hoc Dunnett's test.

3.12 The anti-photoaging effect of HRF-loaded PLGA nanoparticles on mouse skin

Then, we developed the HRF (Harak formula) and and its bioactive hispidulin (HPD)-loaded polylactide-co-glycolide (PLGA) nanoparticles (HRF-NPs and HPD-NPs, respectively) and investigated their anti-photoaging effects compared to free HRF and HPD controls through the inhibition of MMP-1 and promotion of collagen in mouse skin. The HRF-NPs and free HRF (7.5, 15, 30 mg/cm²) as well as HPD-NPs and free HPD (2.5, 5, 10 mg/cm²) significantly protected against UVA (8 J/cm²)-induced ROS generation in NHDFs (Fig. 16). Moreover, topical administration of HRF-PLGA-NPs and free HRF at 5, 15, 50 mg/cm² as well as HPD-PLGA-NPs and free HPD at 6, 20, 60 mg/cm² 1 h prior to UVA exposure (3 times (10 J/cm²)/week up to 2 weeks; accumulation dose 60 J/cm²) reversed UVA-dependent an increase in MMP-1 protein expression (Fig. 17) and a decrease in collagen type I protein expression (Fig. 18) in mouse skin. In addition, at an equal amount of the compound mass, less quantity of HRF by approximately 50% in nanoparticle-based formulation compared to free HRF formula had abilities to suppress UVA-induced skin photoaging in association with inhibition of cellular oxidant formation.

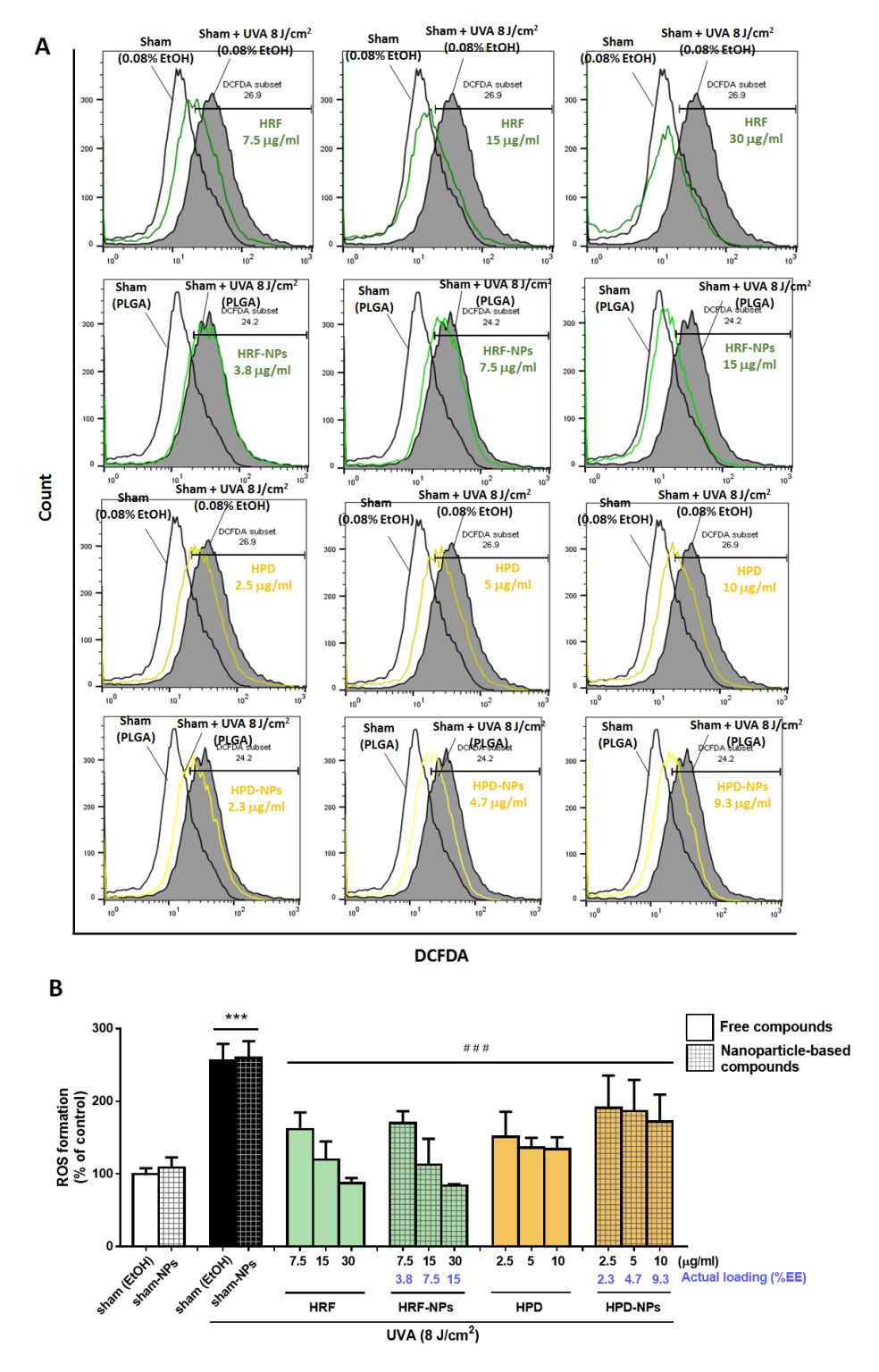


Figure 16. HRF-NPs and HPD-NPs protect against UVA-induced ROS formation. Normal human dermal fibroblasts (NHDFs) were treated with HRF-NPs and HPD-NPs or controls (free HRF and HPD, respectively) prior to UVA (8 J/cm²) irradiation. (A) Flow cytometry histograms of DCFDA fluorescence. (B) The mean fluorescence intensity of the DCFDA staining with regard to the background level of untreated cells (sham control). Data shown are mean \pm s.d. of at least three biological replicates ($n \ge 3$) performed on different days in duplicate. *** P < 0.001 c.f. the sham-irradiated groups, ### P < 0.001 c.f. UVA treatment, one-way ANOVA with post-hoc Dunnett's test.

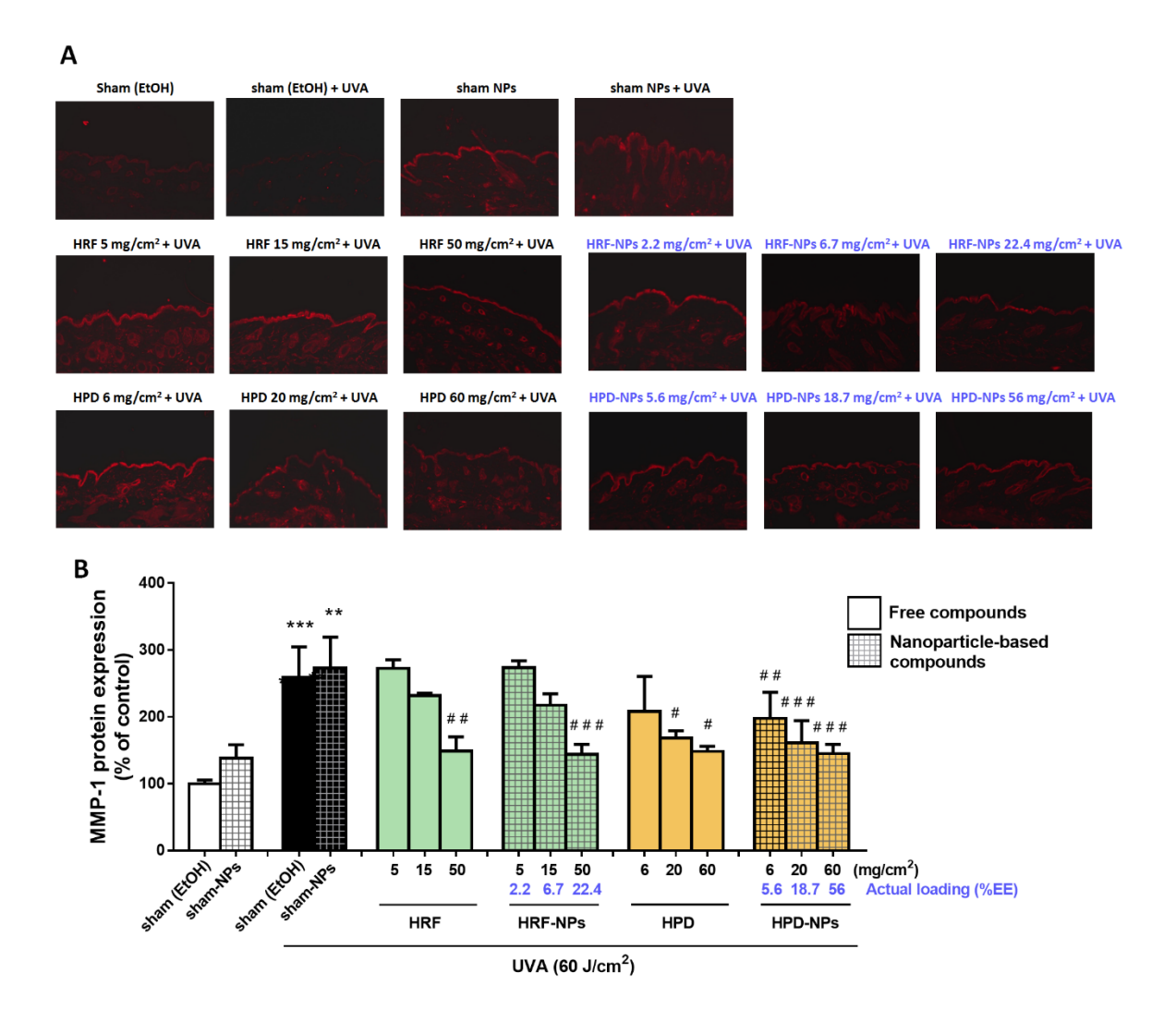


Figure 17. The protective effects of HRF-NPs and HPD-NPs and the free compound controls on UVA-induced MMP-1 induction in mouse skin. BALB/c mice were topically applied with 5, 15, and 50 mg/cm² HRF-NPs and free HRF control as well as 6, 20, and 60 mg/cm² HPD-NPs and free HPD control on the dorsal skin for 1 h prior to each UVA irradiation (10 J/cm²/session 3 times a week for 2 weeks; a cumulative total dose of 60 J/cm²). (A) The fluorescence imaging of MMP-1 in mouse skin collected at 24 h following the last UVA exposure. (B) The summary graph with the statistical analysis of the protein levels of MMP-1 quantified by ImageJ and GraphPad Prism software. Data was shown as mean \pm SD at the 20X magnification (scale bar = 50 mm), n = 4. **P < 0.01, ***P < 0.001 versus non-irradiated sham group by Student's t-test. *P < 0.05; *P < 0.01; *P < 0.001 versus the sham-irradiated group by one-way ANOVA Dunnett's test.

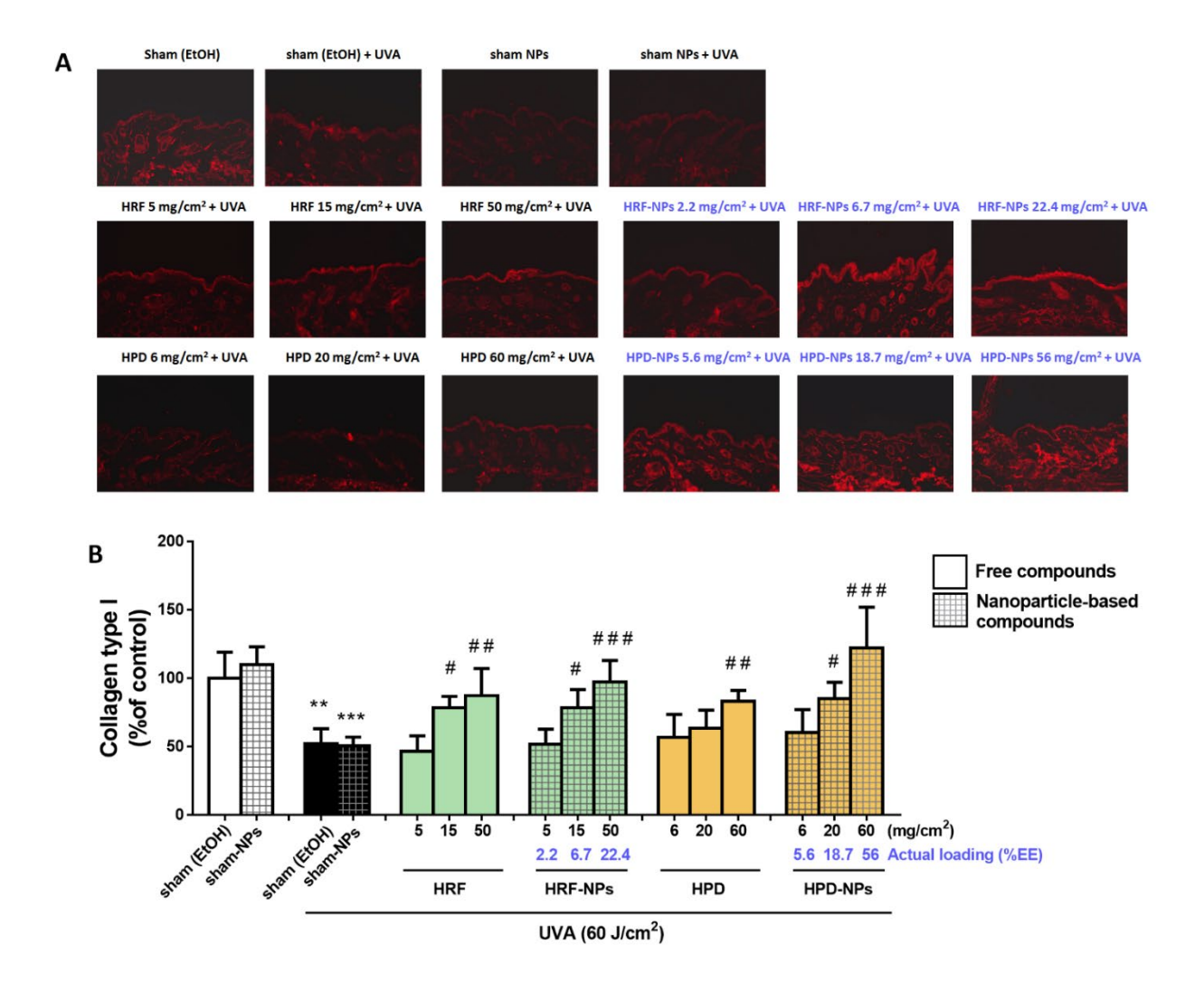


Figure 18. The protective effects of HRF-NPs and HPD-NPs and free HRF and HPD controls on UVA-induced collagen depletion in mouse skin. BALB/c mice were topically applied with HRF-NPs (5, 15, and 50 mg/cm²), HPD-NPs (6, 20, and 60 mg/cm²) and the free HRF and HPD controls on the dorsal skin for 1 h prior to each UVA irradiation (10 J/cm²/session 3 times a week for 2 weeks; a cumulative total dose of 60 J/cm²). (A) The fluorescence imaging of collagen type I in mouse skin collected at 24 h following the last UVA exposure. (B) The summary graph with the statistical analysis of the protein levels of collagen type I quantified by ImageJ and GraphPad Prism software. Data was shown as mean \pm SD at the 20X magnification (scale bar = 50 mm), n = 4. **P < 0.01, ***P < 0.001 versus non-irradiated sham group by Student's t-test. *P < 0.05; **P < 0.01; **P < 0.001 versus the sham-irradiated group by one-way ANOVA Dunnett's test.

Executive Summary (สรุปผลการทดลอง)

Ultraviolet radiation (UVR) plays a role in skin photodamage through triggering various biological responses of skin cells including apoptosis, oxidative stress and melanogenesis. We previously reported that human epidermal keratinocytes (KC) exerted paracrine protective effects on UVB-induced DNA damage and apoptosis in melanocytes (MC). We thus determined the protective paracrine effects of 5 skin cell types including KC, human keratinocyte cell line (HaCaT), primary human dermal fibroblasts (HDF), mouse fibroblast cell line (NIH3T3) and epidermoid carcinoma (A431) on UVB-induced MC responses. The results showed that conditioned medium (CM) from 4 types of the skin cells except A431 cells reduced caspase-3 activation and ROS formation induced by UVB (250 and 62.5 mJ/cm², respectively) as well as increased tyrosinase activity and melanin level in MC exposed to UVB (125 mJ/cm²). KC provided the highest modulatory effects on UVB-induced caspase-3 activation, oxidant formation and melanogenesis in MC. We next identified the candidate genes encoding paracrine factors (PF) in KC and HaCaT responsible for their protective effects on UVB-mediated MC responses using RNA-seq. The results revealed that UVB caused a significant expression of 48 paracrine factor genes in UVB (125 mJ/cm²) treated KC and HaCaT cells compared to unirradiated cells. Moreover, 16 up-regulated transcripts in both KC and HaCaT were identified after UVB irradiation. We observed that 7 important paracrine factor genes including CCL20, TNFRSF10D, GCSF, IL6, IL36G, CXCL2, CXCL8 were significantly upregulated in UVB-treated KC which provide the strongest modulatory effects on UVB-induced MC responses more than UVB-treated HaCaT cells. In addition, to identify a correlation between the rescue activity of candidate paracrines and their corresponding transcripts expressed in KC, GCSF and CCL20 were observed to provide the strongest modulatory effects on the MC responses (apoptosis, melanogenesis and ROS production). Exposure of KC to UVB led to a substantial increase in secretion of GCSF, corresponding to the concentrations of the recombinant proteins having the biological effects on MC. To demonstrate the in vivo relevance of the in vitro findings, immunofluorescence analysis revealed a correlation between expression of GCSF and CCL20 proteins in epidermis and of the major melanogenic enzyme tyrosinase, an indicative of the MC responses in mouse skin exposed to UVB irradiation. Our study therefore suggested that the GCSF and CCL20 may be candidate paracrine factors secreted from KC that contribute to a regulatory role on the stress responses of MC to UVB.

Since mitochondria are the major source of oxidant production as well as key sources of cellular oxidants during UVA exposure, we also evaluated the effects of two potent novel mitochondria-targeted H_2S delivery molecules (AP39 and AP123) in UVA-induced photoaging. Indeed, both compounds (but not their respective non-targeted controls) decreased UVA-induced

oxidative stress, MMP-1 induction and collagen degradation, prevented UVA-induced loss cellular bioenergetics and increased mitochondrial ETC (electron transport chain) activity and ATP synthesis with concomitant increases in Nrf2 nuclear accumulation and its target gene levels in normal human dermal fibroblasts. These findings were generally reproduced *in vivo* and both compounds (but not their respective controls), dose-dependently decreased MMP-1 induction, collagen loss and oxidative DNA damage. AP39 and AP123 also induced a significant Nrf2 activation in mouse skin, concomitant with upregulation of cytoprotective defense enzymes GST, NQO-1 mitochondrial MnSOD and increased mitochondrial biogenesis, presumably through preserving mitochondrial bioenergetics preventing mitochondrial oxidant production and preserving subsequent downstream Nrf2 signalling.

We also performed the mouse model of skin aging to demonstrate the in vivo relevance to the in vitro anti-photoaging effects of potential natural compounds and herbal products. We have observed that HRF extracts and their potential bioactive compound HSP prevented UVA-induced photoaging of mouse skin in vivo via suppressing oxidative damage and downregulating MMP-1mediated collagen degradation through the regulation of cytoprotective Nrf2 activity. Furthermore, we developed the PLGA-based nanoparticles incorporated with the HRF and then investigated the anti-photoaging effects of HRF-NPs compared to free HRF control through the inhibition of ROS generation in NHDFs as well as reduction of MMP-1 and increasing of collagen in mouse skin. At an equal amount of the compound mass, less quantity of HRF in nanoparticle-based formulation compared to free HRF control significantly protected against UVA (8 J/cm²)-induced ROS generation in NHDFs. Moreover, topical administration of nanoparticle-based HRF 1 h prior to UVA exposure (3 times (10 J/cm²)/week up to 2 weeks; accumulation dose 60 J/cm²) attenuated epidermal thickness and MMP-1 protein expression as well as increased collagen type I protein expression in UVA-induced mouse skin. Our observations revealed that, at an equal amount of the compound mass, less quantity of HRF by approximately 50% in nanoparticle-based formulation compared to free HRF formula had abilities to suppress UVA-induced skin photoaging in association with inhibition of cellular oxidant formation.

Our study concludes that the microenvironment created by KC played a regulatory role on the stress responses of MC to UVB via paracrine actions mediated by GCSF and CCL20. The UVB-responsive genes in KC may be promising in developing UVB biomarkers for predicting susceptibility of the skin to photodamage. Promotion of Nrf2 activity by medicinal plants (HRF extracts) and their bioactive compounds (e.g., HSP, HPD) as well as targeting H₂S delivery to mitochondria may represent a promising pharmacological strategy for the prevention and treatment of skin photoaging. Furthermore, PLGA nanoparticles improved the efficiency of HRF in protection against UVA-induced

skin photoaging and the HRF encapsulated in PLGA-based nanoparticles may represent promising anti-photoaging candidates. Further investigations on clinical efficacy and safety are required to develop of the HRF encapsulated in PLGA-based nanoparticles as promising anti-photoaging agents.

Output จากโครงการวิจัย

- ผลงานตีพิมพ์ในวารสารวิชาการนานาชาติ (ระบุชื่อผู้แต่ง ชื่อเรื่อง ชื่อวารสาร ปี เล่มที่ เลขที่ และหน้า)
 หรือผลงานตามที่คาดไว้ในสัญญาโครงการ
 - 1.1 Lohakul J, Chaiprasongsuk A, Jeayeng S, Saelim M, Muanjumpon P, Thanachaiphiwat S, Tripatara P, Soontrapa K, Lumlerdkij N, Akarasereenont P, Panich U. The Protective Effect of Polyherbal Formulation, Harak Formula, on UVA-Induced Photoaging of Human Dermal Fibroblasts and Mouse Skin via Promoting Nrf2-Regulated Antioxidant Defense. Front Pharmacol. 2021 Apr 12;12:649820. (SJR Quartile: Q1 Impact factor: 5.81)
 - 1.2 Lohakul J, Jeayeng S, Chaiprasongsuk A, Torregrossa R, Wood M.E, Saelim M, Thangboonjit W, Whiteman M, Panich U. Mitochondria-targeted hydrogen sulfide delivery molecules protect against uva-induced photoaging in human dermal fibroblasts, and in mouse skin in vivo. Antioxid Redox Signal. 2022 Jun;36(16-18):1268-1288. (SJR Quartile: Q1 Impact factor: 8.4)
 - 1.3 Chaiprasongsuk A, Panich U. Role of Phytochemicals in Skin Photoprotection via Regulation of Nrf2. Front Pharmacol. 2022 May 12;13:823881. (SJR Quartile: Q1 Impact factor: 5.81)
- 2. การนำผลงานวิจัยไปใช้ประโยชน์

เชิงวิชาการ:

- มีการพัฒนาการเรียนการสอน ผลิตนักศึกษาบัณฑิตศึกษาระดับปริญญาเอก 1 คนและพัฒนา นักวิจัยหลังปริญญาเอกให้มีความเชี่ยวชาญในการใช้เทคโนโลยีด้านเภสัชวิทยาเชิงระบบและเชิง ลึกในการคันพบ biomarkers ใหม่เพื่อต่อยอดสู่ศาสตร์ด้าน precision dermatology
- สร้างความเข้มแข็งด้านเครือข่ายวิจัยกับ Professor Matthew Whiteman, University of Exeter Medical School ประเทศอังกฤษ โดยผลงานวิจัยยังได้รับการเผยแพร่ในสื่อสิ่งพิมพ์หลายแหล่ง ของต่างประเทศ ได้แก่ https://www.gccbusinessnews.com/newly-discovered-drug-molecules-block-age-related-skin-issues-from-sun-exposure/, https://breakthrough.neliti.com/slip-slop-slap-and-swallow-new-molecules-may-prevent-skin-ageing-from-sun-exposure/, https://topic.echemi.com/a/new-drug-molecules-can-prevent-skin-aging-caused-by-sun-exposure_177151.html,

https://www.dailyadvent.com/news/9222643cb14ace07aa35ca6f2acbc554-Two-New-Drugs-Could-Prevent-Skin-Aging-Caused-by-Sun,https://detonic.shop/news/new-drug-molecules-could-prevent-skin-aging-caused-by-sun-exposure/

การจดสิทธิบัตร

ชื่อสิ่งประดิษฐ์: กระบวนการผลิตอนุภาคนาโนสำหรับนำส่งสารต้านอนุมูลอิสระ 3 คำขอ

เลขที่คำขอ: 2101008241
 เลขที่คำขอ: 2101008253
 เลขที่คำขอ: 2101008256

ลงนาม.....(รศ. ดร. พญ.อุไรวรรณ พานิช)
(หัวหน้าโครงการวิจัยผู้รับทุน)

